9th International Conference on Vortex Flow Mechanics

ICVFM 2021

11-13 October 2021, Virtual Conference,
University of Patras, Greece

Final Programme

Book of Abstracts

Virtual Conference Guidelines

9th International Conference on Vortex Flow Mechanics ICVFM 2021

11-13 October 2021, Virtual Conference,
University of Patras, Greece

Vortices play a dominant role in fluid dynamics. Besides their fascinating shape and structure, they are important in many physical phenomena and technological applications and may require special tools for their analysis and experimental or numerical study. Mastering vortex dynamics and modeling is relevant for both fundamental and applied sciences. Understanding vortex dynamics is key to solve multiscale problems in turbulence, to predict unsteady loadings on engineering devices, to forecast the weather, etc.

The scope of the series of the International Conferences on Vortex Flow Mechanics is to provide a platform for scientists and engineers to present state-of-the art research and discuss recent developments in the field of vortex physics, modeling, and applications. This series of successful meetings commenced in Kobe in 1999 and continued in Istanbul (2001), Yokohama (2005), Daejeon (2008), San Leucio (2010), Nagoya (2014), Rostock (2016), and Xi'an (2018).

The 9th International Conference on Vortex Flow Mechanics, originally planned to take place in 2020, in Patras, Greece, has suffered the difficulties of the COVID-19 pandemic. Postponed to October 2021, due to ongoing COVID-19 concerns, the conference is organized by the University of Patras as a virtual conference held entirely online from 11th to 13th October 2021.

The conference covers but is not limited to the following topics:

- Turbulent flow
- Multiphase flow
- Reacting flow
- Free-shear flow
- Stratified flow
- Bio-fluid mechanics
- Computation fluid mechanics
- Flow measurements
- Flow control
- Turbomachinery
- Aero-acoustics
- Aerodynamic design optimization
- Flow-induced vibration
- Microfluidics
- Scientific visualization methods
- Vortex dynamics in ship hydromechanics

9th International Conference on Vortex Flow Mechanics ICVFM 2021

11-13 October 2021, Virtual Conference,
University of Patras, Greece

Organizing Committee

Chair
Prof. Thrassos Panidis, University of Patras, Greece
Vice-Chair
Prof. Xiande Fang, Nanjing University of Aeronautics and Astronautics, China
Members
Prof. Yannis Kallinderis, University of Patras, Greece
Prof. Dionyssios Margaris, University of Patras, Greece
Prof. Spyros Voutsinas, National Technical University of Athens, Greece
Prof. Kyros Yakinthos, Aristotle University of Thessaloniki, Greece
Secretary
Dr. Alexandros Romeos, University of Patras, Greece

Executive Committee

Prof. Hikaru Aono, Tokyo University of Science, Japan
Prof. Keh-Chin Chang, Cheng Kung University, Taiwan China
Prof. Bin Chen, Xi'an Jiaotong University, China
Prof. Galina Dynnikova, Moscow State University, Russia
Prof. John Ekaterinaris, Embry-Riddle Aeronautical University, FL USA
Prof. Masaki Fuchiwaki, Kyushu Institute of Technology, Japan
Prof. Hitoshi Ishikawa, Tokyo University of Science, Japan
Prof. Kyoji Kamemoto, Yokohama National University, Japan
Prof. Nikolai Kornev, University of Rostock, Germany
Prof. Petros Koumoutsakos, ETH Zurich, Switzerland
Prof. Jiun-Jih Miau, National Cheng Kung University, Taiwan China
Prof. Iraj Mortazavi, Institute Polytechnique de Bordeaux, France
Prof. Andrew Pollard, Queen's University, Kingston, ON Canada
Prof. Alexei Setukha, Moscow State University, Russia
Prof. Tomomi Uchiyama, Nagoya University, Japan
Prof. Gregoire Winckelmans, Université Catholique de Louvain, Belgium
Prof. Xiaogang Yang, The University of Nottingham, UK
Prof. Yoshifumi Yokoi, National Defense Academy of Japan, Japan

ICVFM 2021

9th International Conference on Vortex Flow Mechanics

11-13 October 2021, Virtual Conference, University of Patras, Greece

Programme Overview

[Reference time zone is that in Patras, Greece (EEST, GMT+3)]

1st Day	**Monday, October 11th, 2021**
11:00-11:20	**Welcome**
11:20-13:20	**SESSION 1**
11:20-12:00	Keynote Presentation Vortex induced vibrations in aerodynamics *Spyros Voutsinas*
12:00-13:20	*Oral presentations*
13:20-13:40	Break
13:40-15:40	**SESSION 2**
13:40-15:40	*Oral presentations*
15:40-16:00	Break
16:00-16:40	**SESSION 3**
16:00-16:40	Keynote Presentation Vortices interacting with smart materials and structures: the case of energy harvesting *Oleg Goushcha/Yannis Andreopoulos*

2nd Day	**Tuesday, October 12th, 2021**
11:00-12:20	**SESSION 4**
11:00-11:40	Keynote Presentation Empirical Predictive Method for Two-Phase Flow Condensation Heat Transfer in Plain Channels *Xiande Fang*
11:40-12:20	Keynote Presentation Flow and Control of Some Jets and Separated Flows *Toshihiko Shakouchi*
12:20-12:40	Break
12:40-14:00	**SESSION 5**
12:20-14:00	*Oral presentations*
14:00-14:20	Break
14:20-16:00	**SESSION 6**
14:20-16:00	*Oral presentations*

3rd Day	**Wednesday, October 13th, 2021**
11:00-13:00	**SESSION 7**
11:00-11:40	Keynote Presentation Mitigating Aircraft Wake Vortex Risks During Final Approach via Plate Lines *Frank Holzäpfel*
11:40-13:00	*Oral presentations*
13:00-13:20	Break
13:30-15:20	**SESSION 8**
13:30-15:20	*Oral presentations*
15:20-15:40	**Closing remarks**

ICVFM 2021

9th International Conference on Vortex Flow Mechanics

11-13 October 2021, Virtual Conference, University of Patras, Greece

Programme

[Reference time zone is that in Patras, Greece (EEST, GMT+3)]

1st Day	Monday, October 11th, 2021
11:00-11:20	Welcome
	SESSION 1 Chair Prof. Nikolai Kornev
11:20-12:00 (S1.K1)	Keynote Presentation Vortex induced vibrations in aerodynamics *Spyros Voutsinas*
12:00-12:20 (S1.1)	Sinusoidally heaving airfoil on an elastic hinge *Yaroslav Dynnikov, Galina Dynnikova, Sergey Guvernyuk and Tatyana Malakhova*
12:20-12:40 (S1.2)	Resonant vortex-wake forces on circular cylinders *Efstathios Konstantinidis*
12:40-13:00 (S1.3)	A Computer Aided Optimizing Design for Drone Rotors *Daichi Yoshidome and Norihiko Watanabe*
13:00-13:20 (S1.4)	On the Vortex Method for Modeling a Separated Flow of an Inviscid Fluid *Alexey Setukha*
13:20-13:40	Break
	SESSION 2 Chair Prof. Thrassos Panidis
13:40-14:00 (S2.1)	Calculation of pressure, force, and moment in meshless vortex methods *Galina Dynnikova*
14:00-14:20 (S2.2)	Interpolating Vortex Particle Methods using Splines Wavelets *Matthias Kirchhart*
14:20-14:40 (S2.3)	Effect of Froude number on the motion of a sphere launched vertically upward in water *Kotaro Takamure and Tomomi Uchiyama*
14:40-15:00 (S2.4)	Analytical Description of the Vortex Ring Induced by a Ring Plume *Maria Stefanidou, Aristeidis Bloutsos, George Horsch, Athanassios Dimas and Panayotis Yannopoulos*
15:00-15:20 (S2.5)	Flow visualization of transitional channel flow with polymer additive *Sattaya Yimprasert, Per Henrik Alfresdsson and Masaharu Matsubara*
15:20-15:40 (S2.6)	Micropolar Theory on Turbulence Modulation *George Sofiadis, Evangelos Karvelas and Ioannis Sarris*
15:40-16:00	Break
	SESSION 3 Chair Prof. Spyros Voutsinas
16:00-16:40 (S3.K1)	Keynote Presentation Vortices interacting with smart materials and structures: the case of energy harvesting *Oleg Goushcha/Yannis Andreopoulos*

2nd Day	**Tuesday, October 12th, 2021**
	SESSION 4 Chair Prof. Bin Chen
11:00-11:40 (S4.K1)	Keynote Presentation Empirical Predictive Method for Two-Phase Flow Condensation Heat Transfer in Plain Channels *Xiande Fang*
11:40-12:20 (S4.K2)	Keynote Presentation Flow and Control of Some Jets and Separated Flows *Toshihiko Shakouchi*
12:20-12:40	Break
	SESSION 5 Chair Prof. Alexei Setukha
12:40-13:00 (S5.1)	Experimental study on the heat transfer characteristics and frequency control of flashing spray cooling under varying operating conditions *Shangming Wang, Zhifu Zhou and Bin Chen*
13:00-13:20 (S5.2)	Influence of the inlet local annular swirling zone on an axisymmetric turbulent jet *Yevhenii Shkvar, Shiju E, Dmytro Redchyts and Svitlana Moiseienko*
13:20-13:40 (S5.3)	Experimental Study on Coaxial Swirling Jets *Andreas Naxakis, Alexandros Romeos, Athanasios Giannadakis and Thrassos Panidis*
13:40-14:00 (S5.4)	Patient-Specific Diastolic Vortex Flow Patterns in the Left Ventricle *Dimitrios Zantzas, Vasileios Gkoutzamanis, Vasiliki Kantartzi, Vasileios Saxpeckidis and Anestis Kalfas*
14:00-14:20	Break
	SESSION 6 Chair Dr. Alexandros Romeos
14:20-14:40 (S6.1)	Hot-wire measurement of asymptotic characteristics of lobed jet flow *Ren Fukui, Mamoru Takahashi, Koichi Tsujimoto, Toshitake Ando, Tishihiko Shakouchi and Ryuichi Momiyama*
14:40-15:00 (S6.2)	Vortex Structure Produced by a Sweeping Jet in a Cross Flow *Masaki Fuchiwaki, Eisei Kobayashi and Surya Raghu*
15:00-15:20 (S6.3)	Supersonic Under-Expanded Reattached Jet with Vortex Region *Tetsuji Ohmura, Toshihiko Shakouchi, Ryota Matsui and Koichi Tsujimoto*
15:20-15:40 (S6.4)	Fundamental Study on Design Methodology of a Solar Car Considering Aerodynamic and Power Generation Performance *Arata Muto, Ichiro Uto, Kota Fukuda, Kouhei Sagawa and Hideki Kimura*
15:40-16:00 (S6.5)	Study on Drag Reduction of Superstructure of Ships and Improvement of Fuel Consumption *Kodai Fukushima, Kota Fukuda, Takao Kashiwagi, Takashi Danno, Koeki Onishi and Koyu Kimura*

3rd Day	Wednesday, October 13th, 2021
	SESSION 7 Chair Prof. Tomomi Uchiyama
11:00-11:40 (S7.K1)	Keynote Presentation Mitigating Aircraft Wake Vortex Risks During Final Approach via Plate Lines *Frank Holzäpfel*
11:40-12:00 (S7.1)	Comparison of Synthetic Inflow Generation Methods for Atmospheric Boundary Layer Flows *Henry Plischka, Johann Turnow and Nikolai Kornev*
12:00-12:20 (S7.2)	Identification and Analysis of vortical structures over an airliner's wing-fuselage junction *Stylianos Adamidis and Nicholas C. Markatos*
12:20-12:40 (S7.3)	Vortex Dynamics Effects on the Development of a Confined Wake and a Channel Flow in a Rectangular Duct Under Identical Inlet Flow Conditions *Ioannis Kalogirou*
12:40-13:00 (S7.4)	The Numerical Simulation of the Vortex Shedding Flow from Two Circular Cylinders of the Parallel Arrangement in the Lock-in State in the Different Mode *Yoshifumi Yokoi*
13:00-13:20	Break
	SESSION 8 Chair Prof. Xiande Fang
13:20-13:40 (S8.1)	Turbulent channel flow past a wall-mounted cuboid *Ariane Neale Ramos Vieira, Hendrik Kuhlmann, Johann Waringer, Carina Zittra, Jan Martini, Simon Vitecek and Stephan Handschuh*
13:40-14:00 (S8.2)	Numerical Investigation of a Backward Facing Step Flow Controlled by a Synthetic Jet *Dionysia Voultsou, Alexandros Romeos, Alexandros Kalarakis and Athanasios Giannadakis*
14:00-14:20 (S8.3)	An experimental study on the wake of a sphere having a uniaxial through-hole *Hayato Kato, Kotaro Takamure and Tomomi Uchiyama*
14:20-14:40 (S8.4)	Vortical systems, generated by Darrieus and Savonius Rotors *Dmytro Redchyts, Svitlana Moiseienko, Yevhenii Shkvar and Shiju E*
14:40-15:00 (S8.5)	The assessment of the impact of turbulence generated by wind turbines planned for construction in close proximity of high voltage power transmission lines on the wind farm location problems *Waldemar Kamrat*
15:00-15:20 (S8.6)	Vortical flows in the wake of bluff bodies and their role in flame anchoring. *Georgios Paterakis, Konstantinos Souflas, Evangelos Panagiotis Mitsopoulos, Eleni Manouskou and Panagiotis Koutmos*
15:20-15:40	Closing remarks

9th International Conference on Vortex Flow Mechanics

ICVFM 2021

11-13 October 2021, Virtual Conference,
University of Patras, Greece

Book of Abstracts

Keynote Lecture

Spyros Voutsinas
Professor
School of Mechanical Engineering
National Technical University of Athens, Greece

Faculty member of the School of Mechanical Engineering at NTUA since 1991. He received his PhD from NTUA on Unsteady Aerodynamics and carried on his career working on Aerodynamics and related topics such as Aeroelasticity and Aeroacoustics. In terms of applications his focus was on Wind Turbines and Helicopters. He has been active in numerous EU-funded projects on these topics, in four of them as coordinator.

Lecture title:
Vortex induced vibrations in aerodynamics

In aerodynamics external flows are often dominated by vorticity which is linked to the vortex structures that are formed in the wake of solid bodies. Such structures induce velocity and therefore pressure variations both back to the body where-from they are released, and to any other body on which they impinge. If in addition the solid body (or configuration) is flexible, then it is quite frequent that flow-structure interaction will lead to vibrations which under certain conditions means at least degradation of the structure or even failure.

From a practical stand point, vortex induced vibrations (VIV) are critical in many applications; e.g. helicopter rotors, wind turbines, risers, nuclear cooling etc. Also, from a theoretical/numerical point of view the topic is quite challenging due to the strong non-linear character of the interaction between the flow and the structure. While there have been important experimental works in this respect, the focus will be on the theoretical/numerical aspect of the topic. In particular, hybrid Eulerian-Lagrangian numerical solvers will be presented together with results from two cases. The method combines conventional CFD (of the finite volume type) close to the boundaries with an underlying "flow carpet" of moving particles. The specific method was first introduced as a "vortex method" but then extended to also treat compressible flows.

In terms of results, the first set, concerns the interaction of two elastically mounted cylinders in close tandem arrangement that are excited by the same flow but oscillate independently. Depending on the external conditions, different wake patterns are formed that lead to different kind of vibrations; a point that will be discussed. The second concerns the aeroelastic behaviour of a helicopter that has its blades flexible. In this respect predictions will be compared to test data taken on a scaled BO105 helicopter in the DNW tunnel.

Sinusoidally heaving airfoil on an elastic hinge

Yaroslav Dynnikov[1*], Galina Dynnikova[1] , Sergey Guvernyuk[1], Tatyana Malakhova[1]
[1]Lomonosov Moscow State University, Institue of Mechanics,
Michurinsky pr. 1, 119192, Moscow, Russia
* Corresponding Author: yaroslav.dynnikov@gmail.com

The aerodynamics of flapping wings, and airfoils, was studied in many works. In [1], it was shown that sinusoidally heaving of an airfoil can produce thrust and lift. More complex combinations of heaving, pitching, and rotation, were studied in the works [2]-[4] and others. They considered the motion of the airfoils obeys a given law. These works show that correlation between these kinds of motion plays a significant role. The optimal values of the phase shifts exist. It is of interest whether the phase shift will provide thrust and lift if the motion of one of the degrees of freedom will occur under the action of hydrodynamic forces and elasticity.

In this paper, we consider the determined heaving and passive pitching of an airfoil on an elastic hinge.

The Flow-Structure Interaction problem is solved. Numerical simulation was carried out using the Vvflow CFD software (https://github.com/vvflow/vvflow/) which is based on the Viscous Vortex Domains method (VVD) [5]. The method VVD is a kind of the diffusion velocity method [6]. The vortex region of the flow is represented by the set of vortex particles (small domains) that move relative fluid at diffusion velocity. New vortex particles are generated at the body surfaces at each time step. The values of the new particles circulation must provide the no-slip boundary conditions. These conditions are written as linear equations relative to these values. This system of equations is supplemented by equations of body dynamics, which are linear to acceleration and the new particle's circulation also. Thus, all unknown quantities are calculated simultaneously without splitting the step into hydrodynamic and dynamic parts.

The axis of the hinge locates on the line of symmetry of the airfoil near the leading edge. It performs harmonic transverse oscillations. The oscillation amplitude A dimensioned by the chord length, Strouhal number Sh, hinge stiffness k, and Reynolds number Re vary. Various types of vortex wakes were obtained. Some of them are asymmetrical (see Fig. 1). In this case, a vertical force occurs, directed opposite deviation of the wake. The reason for the loss of symmetry is the instability of the reverse vortex street. This phenomenon is explained by work [7].
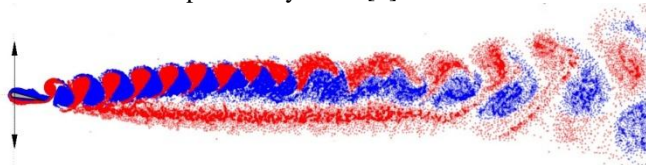
Fig. 1: The vortex wake behind the airfoil at $A = 0.2$, Sh = 2, $k = 10$, Re = 200, $\rho = \rho_f$.

It is shown that in all the cases considered, there is an optimal value of the stiffness of the hinge at the remaining parameters fixed. In this case, the thrust of a rigidly fixed airfoil is lower than at the optimal stiffness value (See Fig. 2). This phenomenon is explained by the fact that when elastically fixing, the airfoil deviates towards a smaller pressure that leads to increasing the horizontal projection of the aerodynamic force in the direction opposite to the flow. Hence, the thrust increases. On the other hand, if the stiffness of the hinge tends to zero, the pressure difference between the two sides of the profile decreases that leads to a decrease in thrust.
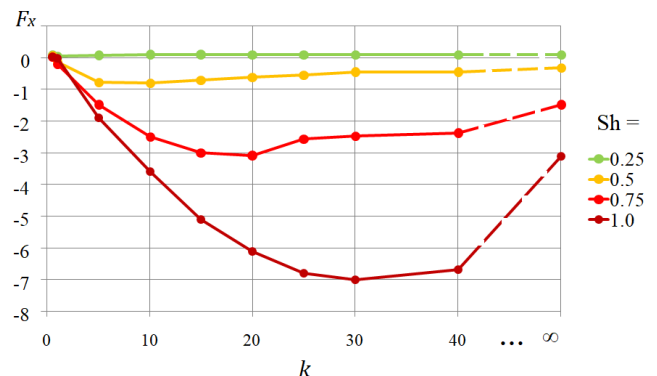
Fig. 2: Drag force dependencies on the hinge stiffness at $A = 0.5$, Re = 200, $\rho = \rho_f$.

References

[1] Jones K.D., Dohring C.M., and Platzer M. F. Experimental and Computational Investigation of the Knoller–Betz Effect. AIAA Journal 1998, **36**(7).

[2] Platzer M.F. and Jones K.D. Flapping-wing aerodynamics: progress and challenges. AIAA Journal 2008, **46**(9).

[3] Floryan D., Van Buren T., Rowley C.W., and Smits A.J., Scaling the propulsive performance of heaving and pitching foils. Journal of Fluid Mechanics 2017, 822, 386.

[4] Haizhou Hu and Yankui Wang. Vertical force generation of a vectorial thruster that employs a rigid flapping panel. Physics of Fluids, 2021, **33** (061906).

[5] Andronov P.R., Dynnikov Y.A., Dynnikova G.Y., and Guvernyuk. S.V. Flow-induced oscillations of circular cylinder in a narrow channel. Aerospace Science and Technology, 2019, **93**(105348):1–5.

[6] Ogami Y. and Akamatsu T. Viscous flow simulation using the discrete vortex model. The diffusion velocity method. Computers and Fluids,1991, **19**(3/4), 433–441.

[7] Dynnikova G.Y., Dynnikov Y.A., Guvernyuk S.V., Malakhova T.V. Stability of a reverse Karman vortex street. Physics of Fluids, 2021, **33**, (024102).

Resonant vortex-wake forces on circular cylinders

Efstathios Konstantinidis[1*]

[1]*University of Western Macedonia, Department of Mechanical Engineering, Bakola & Sialvera, 50132, Kozani, Greece*
* Corresponding Author:ekonstantinidis@uowm.gr

The fluid loading on bluff bodies depends strongly on the wake being at a resonant state, which may occur when the flow is excited by some external disturbance, or when the body undergoes flow-induced vibration. Modeling and prediction of the flow-induced forces on bluff bodies still poses a major challenge because different physical mechanisms are not fully accounted for. In this study, we attempt to shed light into these mechanisms by looking into the elemental- volume contributions of the vorticity to the integrated forces on a circular cylinder using the decomposition by Chang [1], which has its origin in the work of Quartapelle and Napolitano [2].

In this study, we consider a fixed body in a time-dependent free stream, a case that provides a generalized framework to uncover the elemental force contributions in resonant wakes. Flow data were produced by two-dimensional simulations using an in-house finite-volume code on an orthogonal curvilinear mesh [3]. The freestream velocity far upstream oscillates harmonically as $U(t) = U_0 + \Delta U \cos(\omega t)$ at a maximum Reynolds number of 180 based on the instantaneous velocity. The problem is described by two dimensionless parameters, i.e. the frequency and velocity ratios

$$\omega_r = \frac{\omega}{4\pi f_{v0}} \qquad \varepsilon_r = \frac{\Delta U}{U_0} \qquad (1)$$

where f_{v0} is the frequency of vortex shedding in steady flow of the same average Reynolds number.

Assuming a potential velocity field $\boldsymbol{u} = \nabla\Phi$ the contribution of vorticity within the fluid to the force acting on the body can be expressed as

$$-\frac{\rho}{U}\int_{V_f} \boldsymbol{u} \otimes \boldsymbol{\omega} \cdot \nabla\Phi \, \mathrm{d}V \qquad (2)$$

where $\boldsymbol{\omega}$ is the vorticity vector and the integral is computed over the entire fluid domain. The integrant quantity represents the elemental-volume force. In two dimensions, we can calculate the elemental-volume forces in the drag and lift directions, δ_{Dv} and δ_{Lv} respectively such that the integrated vortex-drag force is given by

$$F_{Dv} = \rho \int_{V_f} \delta_{Dv} \, \mathrm{d}V \qquad (3)$$

and the integrated vortex-lift force is given by

$$F_{Lv} = \rho \int_{V_f} \delta_{Lv} \, \mathrm{d}V \qquad (4)$$

It should be noted that the fluid forces also include contributions from inviscid inertia and skin friction (for details see [1]).
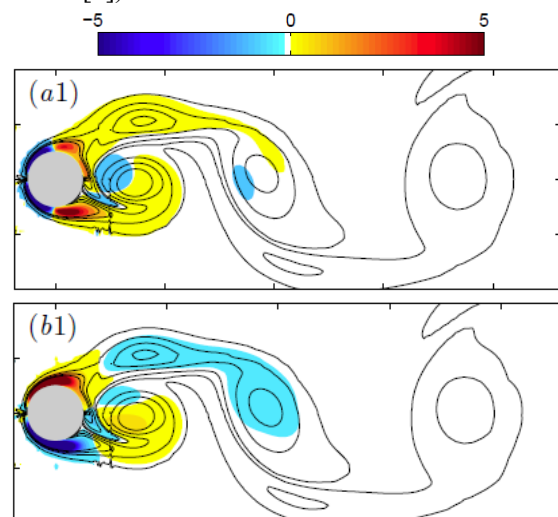
Fig. 1: Contour lines of planar vorticity juxtaposed with elemental-volume force distributions of (*a*1) drag δ_{Dv} and (*b*1) lift δ_{Lv}. Values are normalized with $\frac{1}{2}\rho U_0^2 d$. Run $(\omega_r, \varepsilon_r) = (0.669, 0.333)$.

Fig. 1 shows the instantaneous distributions of δ_{Dv} and δ_{Lv} in the resonant wake at relatively high amplitude. It can be seen that high δ_{Dv} and δ_{Lv} values appear in the region of attached flow around the surface whereas the contribution of wake vortices decreases rapidly with the distance from the body. By analyzing several snapshots over the entire cycle of vortex shedding, we see the variation of elemental force contributions from different flow regions and can explain the origin of double peaks in the time history of the lift force. There is one component that scales with $\sim U(t)$ and another one whose phase is determined by the timing of vortex shedding. Furthermore, the present results gives credence to the in-line force (drag) model proposed recently in [4].

References

[1] Chang, C. C. Potential flow and forces for incompressible viscous flow. Proceedings of the Royal Society of London. Series A: Mathematical and Physical Sciences, 1992, 437: 517-525.

[2] Quartapelle, L., Napolitano, M. Force and moment in incompressible flows. AIAA Journal 1983, 21: 911-913.

[3] Konstantinidis, E., Bouris, D., Vortex synchronization in the cylinder wake due to harmonic and non-harmonic perturbations. Journal of Fluid Mechanics, 2016, 804:248-277.

[4] Konstantinidis, E., Dorogi, D., Baranyi, L. Resonance in vortex-induced in-line vibration at low Reynolds numbers. Journal of Fluid Mechanics, 2021, 907: A34.

A Computer Aided Optimizing Design for Drone Rotors

Daichi Yoshidome[1]*, Norihiko Watanabe[1]

[1]*Sojo University, Ikeda 4-22-1, Kumamoto City, 860-0082, Japan*
* Corresponding Author: nwatanabe@mec.sojo-u.ac.jp

In recent years, the use of drones (Multirotor UAV) has been promoted mainly for industrial use. The field of application of drone will be expanded further with the development of infrastructure and legislation in the future. For that way, it will be necessary to design drones in consideration of various factors depending on the environment, and design costs are expected to increase. Therefore, the more flexible and efficient design method might be required for the design of drones in the future, and one of the effective methods would be a design method that combines numerical optimization technology and CFD which has been used in various situations regardless of the field.

In this study, a design of drone rotor using numerical optimization based on the CFD is performed. Assuming the application of a drone in a residential environment, the rotor shape was attempted to design that can be silent while maintaining as high a lift as possible by choosing the lift and aerodynamic noise as objective functions.

The design optimization sequence of this study is shown in Fig. 1, the rotor to be optimally designed is the rotor of Holy Stone's HS110D, a hobby drone.
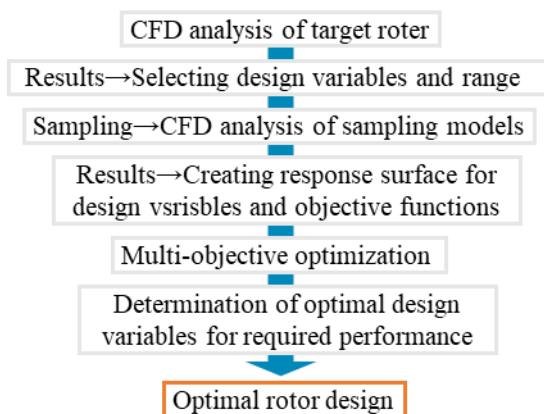
Fig. 1: Flowchart of design optimization

In this study, the SPL (Sound Pressure Level) was used to evaluate the aerodynamic noise. In the CFD analysis, the Proudman model[1], which can calculate the SPL from the amount of turbulence characteristics, was used. The magnitude of the aerodynamic noise was evaluated by the volume of space with an SPL of over 40 dB as shown as light-blue isosurface in Figure 2. In the numerical optimization, the design variables were the angle of attack and warp of the middle wing section and the angle of attack of the outer edge wing section. The objective function was set to be the lift force and the aerodynamic noise, and it was a multi-objective optimization problem to search for the condition that maximized lift and minimized aerodynamic noise.
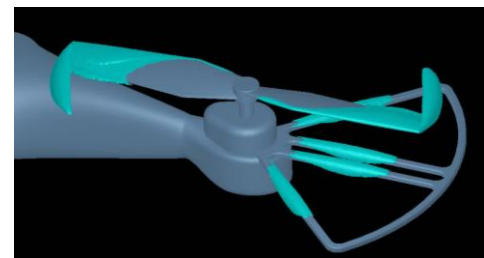
Fig. 2: A space having a sound source over 40 dB

The optimal solution distribution obtained in this study is shown in Fig. 3. In the graph, the horizontal axis is the lift force and the vertical axis is the noise level. The points on the graph are the 1024 best candidate solutions obtained as a result of multi-objective optimization, and as the color changes from red to green to blue, the solution becomes more optimal for the objective.
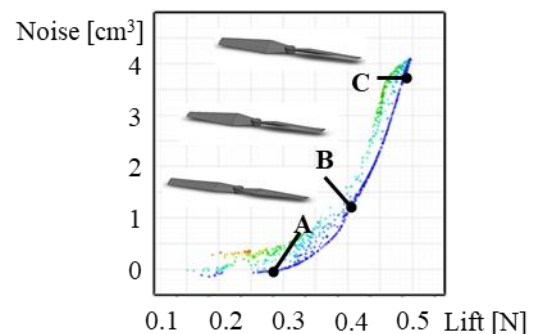
Fig. 3: The pareto solutions

In this paper, three optimal solutions A, B, and C with significantly different performance as shown in Fig. 3 are selected from the optimal solution distributions obtained by optimization, and a discussion of the relationship between the design parameters and the objective function is made from fluid phenomena. As a result, it was found that the parameters of the angle of attack of the middle wing section in particular are involved in all the main phenomena that cause noise, and their contribution to the objective function is high compared to other design variables. Also, the experimental confirmation results will be shown and discussed.

References
[1] Proudman, I., "The generation of noise by isotropic turbulence", Proceedings of the Royal Society of London, A214, (1952), pp. 119-132.

On the Vortex Method for Modeling a Separated Flow of an Inviscid Fluid

Alexey Setukha

Research Computer Centre, Lomonosov Moscow State University, Leninskie Gory, 1, building 4, Moscow, 119234
setuhaav@rambler.ru

A Lagrangian mathematical model of the separated flow of an inviscid incompressible fluid around body with the generation of vorticity on the entire surface of the body is constructed. In this model, an inviscid fluid is treated as the limiting case of a viscous fluid with the Reynolds number tending to infinity.

Consider a flow with constant free-stream velocity $\mathbf{w}_\infty$ and pressure p_∞. Assume that the boundary of the body is a smooth closed surface Σ. The mathematical model is based on the continuity equation and the vorticity transport equation in a viscous fluid:

$$\operatorname{div}\mathbf{w} = 0 , \quad \frac{\partial\boldsymbol{\omega}}{\partial t} + \operatorname{curl}\big[\boldsymbol{\omega}\times\mathbf{w}\big] = \frac{1}{\mathrm{Re}}\Delta\boldsymbol{\omega} , \qquad (1)$$

where $\mathbf{w} = \mathbf{w}(x,t)$ - is the flow velocity , $\boldsymbol{\omega} = \operatorname{curl}\mathbf{w}$ - the vorticity, t is time; x denotes points of space.

Using the relations

$$\Delta\boldsymbol{\omega} = -\operatorname{curl}\operatorname{curl}\boldsymbol{\omega} = -\operatorname{curl}\left[\frac{\boldsymbol{\omega}\times[\operatorname{curl}\boldsymbol{\omega}\times\boldsymbol{\omega}]}{\boldsymbol{\omega}^2} + \frac{\boldsymbol{\omega}\big(\operatorname{curl}\boldsymbol{\omega},\boldsymbol{\omega}\big)}{\boldsymbol{\omega}^2}\right],$$

we can rewrite equation (1) in the following form:

$$\frac{\partial\boldsymbol{\omega}}{\partial t} + \operatorname{curl}\big[\boldsymbol{\omega}\times\mathbf{u}\big] = \frac{1}{\mathrm{Re}}\operatorname{curl}\frac{\boldsymbol{\omega}\big(\operatorname{curl}\boldsymbol{\omega},\boldsymbol{\omega}\big)}{\boldsymbol{\omega}^2} , \qquad (2)$$

$$\mathbf{u} = \mathbf{w} + \mathbf{w}' , \quad \mathbf{w}' = \frac{1}{\mathrm{Re}}\frac{\operatorname{curl}\boldsymbol{\omega}\times\boldsymbol{\omega}}{\boldsymbol{\omega}^2} .$$

The vector field $\mathbf{w}'$ is known as the diffusion velocity. The velocity $\mathbf{u}$ is called the vorticity transport velocity.

Next, we use boundary layer approximation, according to which viscosity plays an important role only in a thin layer on the body surface, while, outside this layer, the viscosity has no effect. This follows from the theory and the boundary layer that the vorticity in the boundary layer is orthogonal to its curl. Therefore, we hypothesize that for large values of the Reynolds number, the right-hand side of equation (2) is negligible (see [1]).

Based on equation (2) with a zero right-hand side, the transition to the Lagrangian description of the flow is carried out. We will consider the laws of motion of particles $x(\xi,t)$, which move with a velocity $\mathbf{u}$, where $\xi = (z,\tau)$ is the Lagrangian coordinate of a particle that was born at a point $z \in \Sigma$ at a moment in time $\tau \geq 0$. We assume that all vorticity is concentrated only in such particles. It is proved that it is possible to introduce the Lagrangian vorticity density $\boldsymbol{\psi}(\xi,\tau)$ so that the fluid velocity is represented as:

$$\mathbf{w}(x,t) = \mathbf{w}_\infty + \int_0^t d\tau \int_{z\in\Sigma_\omega(\tau,t)} \boldsymbol{\psi}(\xi,t)\times\mathbf{V}(x - x(\xi,t))d\sigma_z ,$$

$$\mathbf{V}(x) = x\big(4\pi\big)^{-1}|x|^{-3} .$$

For a pair of functions $x(\xi,t)$ and $\boldsymbol{\psi}(\xi,\tau)$, a complete system of equations is constructed

$$\frac{\partial x(\xi,t)}{dt} = \mathbf{u}(x(\xi,t),t) , \qquad (3)$$

$$\frac{\partial\boldsymbol{\psi}(\xi,t)}{\partial t} = \big(\boldsymbol{\psi}\nabla\big)\mathbf{u} \qquad (4)$$

$$x(\xi,\tau) = z , \quad \boldsymbol{\psi}(\xi,\tau) = \boldsymbol{\gamma}(z,\tau)$$

where $\boldsymbol{\gamma}$ denotes the vorticity flux density on the body surface Σ:

$$\boldsymbol{\gamma}(z,\tau) = \boldsymbol{\omega}(z,\tau)\big(\mathbf{u}(z,\tau)\mathbf{n}(z)\big) , \quad \tau\in[0,T] , z\in\Sigma ,$$

the function $\gamma(z,\tau)$ is a solution of the equation

$$-\frac{1}{2}\mathbf{n}(x)\times\boldsymbol{\gamma}(x,t) + \int_\Sigma \boldsymbol{\gamma}(z,t)\times\mathbf{V}(x - z)d\sigma_z = \mathbf{f}(x,t) , \quad x\in\Sigma ,$$

$$\mathbf{f}(x,t) = -\lim_{\Delta t\to 0}\int_0^{t-\Delta t} d\tau\int_\Sigma \frac{\boldsymbol{\psi}(\xi_z,t')\times\mathbf{V}(x - x(\xi_z,t'))\big|_{t'=t-\Delta t}^{t}}{\Delta t}d\sigma_z$$

Given mathematical model can be used as a theoretical basis for refining and developing some classes of vortex numerical methods. Own version of the numerical scheme based on the discretization of the written equations was built, under the hypothesis is accepted that after its formation, each vortex particle immediately leaves the viscous boundary layer. Therefore, the viscosity initiated the formation of a vortex particle, and its motion occurs in accordance with equations (3)-(4), in which we neglect the diffusion velocity and assume that $\mathbf{u} = \mathbf{w}$.

The method is tested on examples of a number of classical problems of separated flow around bodies.
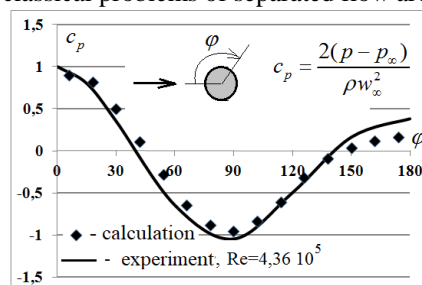
Fig. 1: Distribution of the pressure coefficient over the surface of a sphere in a separate flow (left) and the instantaneous shape of vortex structures (right).

References

[1] Setukha A.V. Lagrangian Description of Three-Dimensional Viscous Flows at Large Reynolds Numbers. Computational Mathematics and Mathematical Physics, 2020, 60(2): 302–326.

Calculation of pressure, force, and moment in meshless vortex methods

Galina Dynnikova

[1]*Lomonosov Moscow State University, Institue of Mechanics,*
Michurinsky pr. 1, 119192, Moscow, Russia
* Corresponding Author: dyn@imec.msu.ru

When simulating incompressible fluid flows by vortex methods, pressure is excluded from the equations. In order to calculate the pressure field or forces acting on bodies, it is necessary to use formulas that express these values in terms of the vorticity and velocity distributions. There are various forms of such expressions in literature. Not all of them are easy to use in vortex meshless methods. Additionally, they are written in continuous form and need an adjustment for use in numerical schemes.

A new general expression of hydrodynamic force exerted on a body is derived in [1] for different boundary conditions (slip, partial slip, no-slip). In this work, a similar expression is obtained for the hydrodynamic moment. The expressions of pressure, force, and moment [1]-[3] are presented in the form adapted for use in numerical meshless vortex methods.

In vortex simulation of flows, researchers deal with a set of discrete vortex elements at each time step. In the translational motion of a body in a viscous fluid under the no-slip boundary condition, all vortex elements represent a vorticity field in the flow region. We will call them free vortices. In the case of an ideal fluid and under the partial slip boundary condition, the model contains the surface vortices, the circulation of which is proportional to the difference between the velocity of the fluid and the body points on its surface. If the body rotates, then the model also contains vortices that simulate the movement of the body. They can be located inside the body or on its surface. These vortices, together with the surface vortices are the so-called attached vorticity. The set of all free and attached vortex elements represents a solenoidal field.

At each time step, all vortex elements are moved/redistributed, and the circulations of new elements are calculated to satisfy the boundary conditions. The new free vortex elements, together with the increments of the attached elements, represent a solenoidal field that induces a velocity field with a single-valued potential $\Delta\varphi$ outside the body. Potential $\Delta\varphi$ is a linear function of the circulation increments $\Delta\Gamma_i^{att}$ of the attached vortex elements, and the circulations Γ_i^{new} of a new free vortex element arisen at current time step Δt.

The following expression for Bernoulli function $B = \dfrac{p}{\rho} + \dfrac{u^2}{2} + H$ is obtained for ideal fluid in the infinite space

$$B(\mathbf{r}) = -\frac{\Delta\varphi}{\Delta t} + \sum_i \mathbf{v}_i(\mathbf{r},\mathbf{r}_i)\cdot\mathbf{w}_i + B_\infty.$$

Here $\mathbf{v}_i$ is velocity induced by the i-th vortex element in the observation point $\mathbf{r}$; $\mathbf{w}_i$ is the movement velocity of the element that is equal to the flow velocity $\mathbf{u}(\mathbf{r}_i)$ for the free

vortex elements and to the body velocity $\mathbf{u}_b(\mathbf{r}_i)$ for the attached vortex elements; H is mass force potential. Expression of Bernoulli function for a viscous fluid in a bounded space is obtained too.

The pressure force expression at arbitrary boundary conditions (no-slip, slip, partial slip) in 3D flow has the form

$$\frac{\mathbf{F}_p}{\rho} = \frac{1}{2\Delta t}\left(\sum_i \Gamma_i^{new}\times\mathbf{r}_i l_i + \sum_i \Delta\Gamma_i^s\times\mathbf{r}_i l_i\right) + V_b\dot{\boldsymbol{\Omega}}\times\mathbf{r}_m$$
$$+ \sum_i\left(\mathbf{u}_{free}-\mathbf{u}_b(\mathbf{r}_i)\right)\times\Gamma_i^s l_i + V_b\ddot{\mathbf{r}}_m.$$

Here l_i is the length of i-th vortex element along the vortex line; $\Gamma_i^s, \Delta\Gamma_i^s$ are circulation of i-th surface vortex element and its increment respectively; $\mathbf{u}_{free}$ is the velocity of the element calculated by the Bio-Savart formula, $\mathbf{r}_m$ is center of mass of the homogeneous body; V_b is its volume, $\boldsymbol{\Omega}$ is angle velocity of the body.

The force and moment expressions are obtained for different kinds of 2D and 3D vortex models at different boundary conditions.
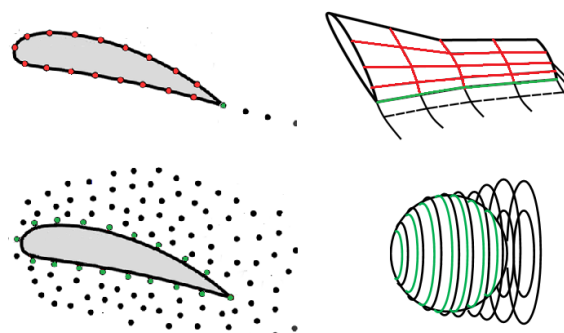
Fig. 1: Some kinds of vortex models. Red and green colors show the attached and new free vortices respectively.

References

[1] Dynnikova G. Y. General expression of aerodynamic force under different boundary conditions (slip, partial slip, no-slip). Physics of Fluids, 2021, **33**(063104).

[2] Dynnikova G. Y. The integral formula for pressure field in the nonstationary barotropic flows of viscous fluid. Journal of Mathematical Fluid Mechanics, 2014, **16**, 145-162.

[3] Dynnikova G. Y., Andronov P. R. Expressions of force and moment exerted on a body in a viscous flow via the flux of vorticity generated on its surface. European Journal of Mechanics, B/Fluids, 2018, **72**, no. Nov-Dec. 293-300.

Interpolating Vortex Particle Methods using Splines Wavelets

Matthias Kirchhart[1*]

[1]Applied and Computational Mathematics, RWTH Aachen University, Schinkelstraße 2, 52066 Aachen, Germany.
*Corresponding Author: kirchhart@acom.rwth-aachen.de

Conventional vortex particle methods interpret a given particle field as a quadrature rule. To obtain a smooth approximation, this quadrature rule is then regularised using so-called blob-functions. The resulting schemes have the advantage of simplicity, but either converge only very slowly or require frequent 'remeshing'.

In this talk we first review our previous work on splines for particle methods. [1] This approach allowed us to perform long-term accurate, high-order simulations without remeshing and could compete with a state-of-the-art discontinuous Galerkin method, see Fig. 1. However, when flows develop steep gradients and particles begin to cluster the method becomes inefficient due to its lack of adaptivity.

We then present a novel approach that instead interprets a given particle cloud as a set of point values and constructs smooth interpolants on them. These interpolants make use of spline wavelets and are adaptive. On the one hand, the method is a natural extension of our previous approach. On the other hand, there is a close relationship with radial basis function interpolants. The resulting schemes have many beneficial properties and preliminary results are promising.

References

[1] Kirchhart M, Rieger C. Discrete Projections: A Step Towards Particle Methods on Bounded Domains without Remeshing. SIAM Journal on Scientific Computing, 2021, 43(1):A609–A635.
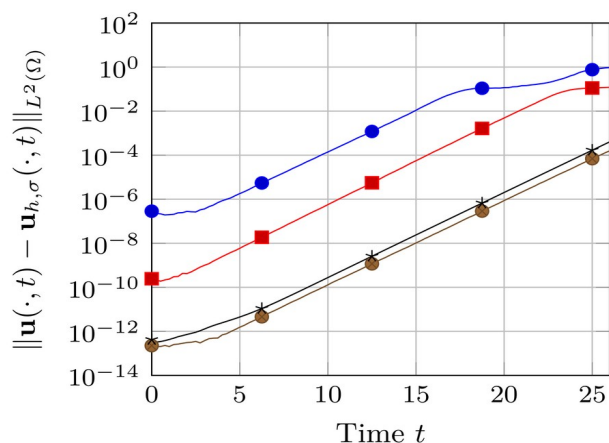
Fig. 1: Error-evolution of 4th, 6th, and 8th-order vortex particle methods using splines on a two-dimensional test-problem without remeshing. [1] Vortex methods using a spline regularisation are competitive with a state-of-the-art discontinuous Galerkin method.

Effect of Froude number on the motion of a sphere launched vertically upward in water

Kotaro Takamure[1*], Tomomi Uchiyama[1]

[1] *Institute of Materials and Systems for Sustainability, Nagoya University, Nagoya, Japan*
* Corresponding Author: kotaro.takamure@imass.nagoya-u.ac.jp

A water exit refers to a situation in which an object is propelled from water into air. The water exit problem is highly complex because it involves nonlinear interference between the object and water surface. In most existing studies on the water exit problem, a primarily symmetrical spherical object was considered to clarify the relevant phenomena [1-2]. Several researches have utilized the Froude number (Fr), which is the ratio of gravity to inertial force, because the water exit is dominated by gravity when the sphere completely passes through the water surface [2-3]. By increasing the water exit velocity, the sphere spends less time submerged in entrained fluid and more time in a gravity-dominated regime. Haohao et al. [2] numerically investigated the effect of Fr ranging as $1.65 < Fr < 8.24$ by using the lattice Boltzmann method, which can effectively capture the large deformations of the air-water interface. Furthermore, Haohao et al. [2] indicated that Fr influenced the rupturing of the interfacial water sheet, which occurred when the sphere passes through the water surface. Thus, it can be considered that because the deformation of the water surface depends on Fr, the interface containing energy must also change accordingly.

To examine this aspect, in this study, a spherical sphere with a density of ρ_p=2640 kg/m^3 and diameter of d=25.4 mm was launched vertically toward the water surface. The value of Fr at the instant in which the sphere crossed the water surface was varied. The dependence of Fr on the sphere motion and water surface behavior was investigated.

An overview of the experimental apparatus is shown in Fig.1(a). The water tank using in this study was a cubic acrylic tank with a side length of 0.4 m. Water was stored in the tank, and a sphere launcher was installed at the center of the bottom of the tank. When the sphere was placed on the launcher, the coordinate origin was the center of the sphere when the sphere was placed in the launcher. The distance from the coordinate origin to the water surface was H, with H=3d for all the considered cases. Fig. 1 shows the schematic of the sphere launch system. When the sphere was placed on the launcher, the iron bar moved vertically downward, thereby compressing the coil spring. When the coil spring was released by pulling the trigger at time t=0, the iron bar moved upward, the small tab at the upper end of the iron bar impacted the sphere, and the sphere was ejected vertically upward. The launch velocity of the sphere was controlled via the compressive displacement of the coil spring.

Fig. 2 shows a snapshot of the instant at which the sphere reaches the maximum displacement position. For Fr = 2.86, a large amount of the water mass is attached around the sphere, and the water surface and sphere are clearly

connected. For Fr = 3.4, a water mass is generated behind the sphere, and a water column is formed between the water surface and the sphere. For Fr = 4.92, most of the water mass separates from the sphere and distributes around the sphere as water droplets. In addition, the water column is elongated but still connects the water surface and sphere. For Fr = 5.9, no water mass is present around the sphere, and the water column is detached in certain regions. These results suggest that a larger Fr corresponds to a smaller influence of the water mass and water column on the sphere at the maximum displacement position of the sphere.
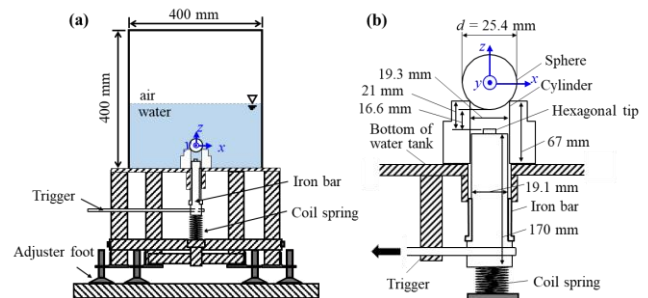
Fig. 1: Schematic of the sphere launch system. (a) Overview of experimental apparatus, (b) details of the launch system.
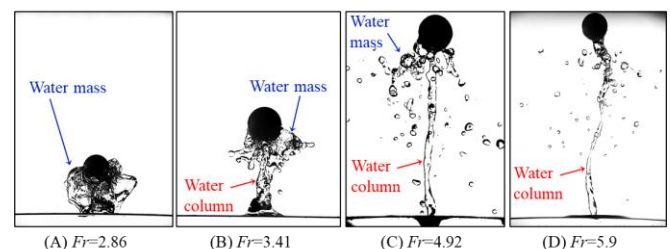
Fig. 2: Behavior of the water mass and water column when the sphere reaches the maximum displacement position.

References
[1] Truscott TT, Epps BP, Munns, et al., Water exit dynamics of buoyant particles, Phys. Rev. Fluids, 2016 1(7): 074501.
[2] Haohao H, Yanping S, et al., Y. Jianyang, Numerical analysis of water exit for a particle with constant velocity using the lattice Boltzmann method, Appl. Ocean Res., 2019 84: 163-178.
[3] Wu Q, Ni B, et al., Experimental study on large deformation of free surface during water exit of a particle, Ocean Eng., 2017, 140: 369-376.

Analytical Description of the Vortex Ring Induced by a Ring Plume

Maria Stefanidou[1*], Aristeidis Bloutsos[1, 3], George Horsch[2], Athanassios Dimas[2] and Panayotis Yannopoulos[1]

[1]*Environmental Engineering Laboratory, Department of Civil Engineering, University of Patras, 265 04 Patras, Greece*
[2]*Hydraulic Engineering Laboratory, Department of Civil Engineering, University of Patras, 265 04 Patras, Greece*
[3]*Hydraulics & Geotechnical Engineering Division, Department of Civil Engineering, University of West Attica, 122 43, Athens, Greece*
* Corresponding Author: stefanidou.m@gmail.com

The ring plume is a buoyant jet discharged vertically with low or without initial inertia and, thus, it is mainly dominated by buoyancy. It may be considered as the limiting case of a rosette-type diffuser with many nozzles discharging fluid into water bodies or in the atmosphere. The fluid may be wastewater, air pollutants or thermal effluents having a little different density than the density of the receiving fluid. The shear flow induced by the velocity right after the exit of the ring nozzle generates a vortex ring occupying the internal diameter of the nozzle. Since the internal diameter of the nozzle includes a solid bottom wall, located at z_0 under the ring exit level, the vortex ring remains stagnant.

In this paper the mathematical analysis of the flow related to a stagnant vortex ring is presented. Following Batchelor [1], for a single circular line vortex of a radius a and strength κ, for the element of integration in the axial plane including the line vortex, the streamlines are described in a cylindrical coordinate system (with the z axis vertical and in coincidence with the vortex ring centreline) by the relationship:

$$\psi(r,z) = \frac{\kappa a r}{4\pi} \int_0^{2\pi} \frac{\cos\theta}{|\vec{s}|} \, d\theta; \tag{1}$$

and the velocities in the r and z direction, respectively, are:

$$u = \frac{\partial\psi}{r\partial z} = -\frac{\kappa a}{4\pi} \int_0^{2\pi} \frac{(z-z_0-a)\cos\theta}{|\vec{s}|^3} \, d\theta \tag{2}$$

$$w = -\frac{\partial\psi}{r\partial r} = -\frac{\kappa a}{4\pi r} \int_0^{2\pi} \frac{[(z-z_0-a)^2+a^2-ar\cos\theta]\cos\theta}{|\vec{s}|^3} \, d\theta, \tag{3}$$

where $|\vec{s}| = [(z-z_0-a)^2 + r^2 + a^2 - 2ra\cos\theta]^{1/2}$. If the vortex has a thin core of radius ε, a rough estimate is $\varepsilon \approx 0.13a$ [1]. Because Eqs. (1)-(3) are valid in an infinite space, while the stagnant vortex occurs in the semi-infinite space, the virtual image technique is applied, according to which a mirrored ring vortex of opposite vorticity is considered. The virtual vortex contributes to the replenishment of quantities lost out of the semi-infinite space.

The strength (or circulation) κ of the ring vortex is constant and independent of the shape of the curve containing the region of vorticity. For the present case, where the vortex ring is generated by the exit ring velocities, κ can be calculated by multiplying the tangential velocity with the perimeter of the maximum radius a of the circular vortex of the vortex ring and a shear stress coefficient c_s. The tangential velocity is considered to be about equal to the exit mean velocity w_0. Therefore, $\kappa = 2\pi a c_s w_0$. For a ring nozzle of a mean radius $R_0 = 6$ cm, the maximum vortex radius is $a = R_0/2 = 3$ cm. Thus, for $w_0 = 0.527$ m/s and $c_s = 0.005$, $\kappa = 5\times10^{-4}$ m²/s and $\varepsilon \approx 0.39$ cm. In the present application, the internal solid bottom level is $z_0 = -0.005$ m. It is necessary that $|\vec{s}| \geq \varepsilon$, which implies that $(z-z_0-a)^2 + (r-a)^2 \geq \varepsilon^2$.

The streamlines and the velocity vector field derived by Eqs. (1)-(3) and using the values of parameters given above are shown in Fig. 1. The upward plume flow velocity field is not depicted in this diagram.
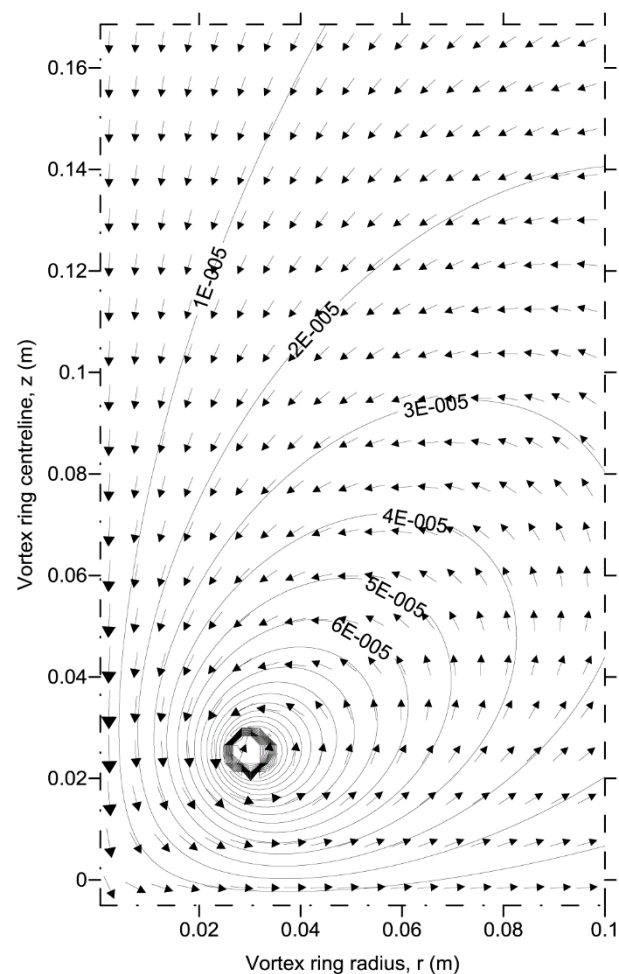
Fig. 1: Vertical cross-section of the vortex ring, showing the streamlines along with the velocity vectors on rz plane, as they are obtained by Eqs. (1)-(3), without the plume flow.

As shown in Fig. 1, the velocity vectors along the vortex ring centreline z, are directed downwards, and they become horizontal just above the solid bottom wall, as expected. In addition, the maximum values of velocities occur on z at the level of the vortex centre.

References

[1] Batchelor, G. K. *An Introduction to Fluid Dynamics*. Cambridge University Press, 2000.

Flow visualization of transitional channel flow with polymer additive

Sattaya Yimprasert[1], P. Henrik Alfredsson[2], Masaharu Matsubara[1*]

[1]*Department of Mechanical System Engineering Shinshu University, Nagano, Japan*
[2]*FLOW, Department of Engineering Mechanics, KTH Royal Institute of Technology, SE-100 44 Stockholm, Sweden*
* *Masaharu Matsubara: mmatsu@shinshu-u.ac.jp*

Drag reduction of internal turbulent water flows by addition of polymers has been widely known as the Toms effect. Furthermore the effect of delaying transition to turbulence has also been reported [1]. In the present study, a polymer, polyacrylamide (PAM), was added to water and flow visualizations around the transition Reynolds number in plane channel flow were performed.

In the experiment, the same water channel flow apparatus as Yimprasert et al. [2] was used. The water channel has a width of $d = 7.1$ mm and a test section length of 4.65 m. At the upstream end of the channel, the Reynolds number was increased by decreasing the spanwise width of the channel, giving a highly disturbed and turbulent flow, the spanwise width was increased and thereby the Reynolds number decreased. In this way, reverse transition from turbulent to laminar flow can be observed in the range of transitional Reynolds numbers. The flow visualizations were performed using reflective flake particles for which the orientation is known to respond to the shear of the flow.

Figure 1 shows the change in the transition Reynolds number due to the addition of PAM. From the visualization photograph, the Reynolds number with intermittent rate (turbulence ratio) γ of 0.2, 0.5, 0.8 was visually determined. Re_s was approximated from the wall friction coefficient C_f obtained from the measured pressure gradient in the channel in the laminar region and calculated as $Re_s = 12/C_f$. Therefore, Re_s can be viewed as an effective Reynolds number defined as $Re_s = U_m d/\nu_e$, where U_m is the average flow velocity, d is the channel width and ν_e an effective viscosity. As can be observed in figure 1 the transition Reynolds number determined for $\gamma = 0.5, 0.8$ clearly increases with increasing polymer concentration C, and also for $\gamma = 0.2$ there is a slight increasing tendency. These results indicate that polymer addition delays the transition to turbulence, which is qualitatively consistent with the results of Chandra et al. [1].

Figure 2 compares the visualization for the case $\gamma = 0.5$. The flow is from left to right. Large streak structures/vortices elongated in the streamwise direction are seen around small-scale turbulent parts, consisting of clusters of fine vortices. This is a characteristic pattern of transitional channel flows of Newtonian fluids [2,3]. In the case with the polymer additive, Figure 2(b), the streaks become longer and the contrast of the streaks in the photograph becomes stronger. The increased contrast can be interpreted as an increase in the shear due to the longitudinal vortices, suggesting that the polymer addition strengthens the longitudinal vortices. These results indicate that the polymer addition does not only delay transition to turbulence but also change the structure of the flow.
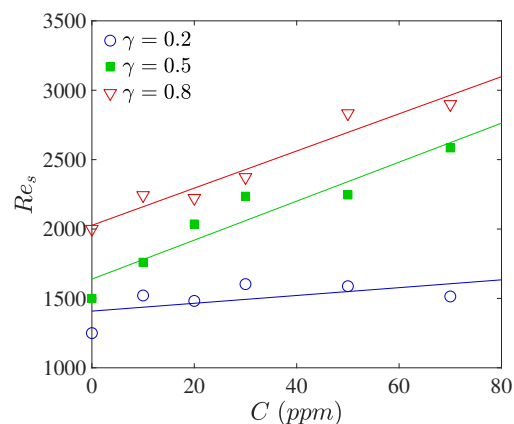
Fig. 1: Transition Reynolds number Re_s versus polymer concentration C.
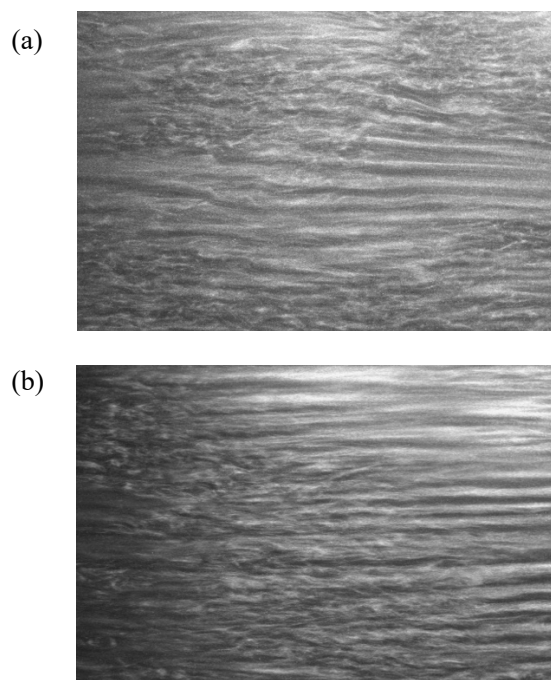
Fig. 2: Flow visualization. (a) water, (b) $C = 70$ ppm.

References

[1] Chandra B, Shankar V, Das, D. Early transition, relaminarization and drag reduction in the flow of polymer solutions through microtubes. Journal of Fluid Mechanics, 2020, 885, A47.

[2] Yimprasert S, Kvick M, Alfredsson PH, Matsubara M. Flow visualization and skin friction determination in transitional channel flow. Exp Fluids, 2021. 62, 31.

[3] Tsukahara T, Seki Y, Kawamura H, Tochio D. DNS of turbulent channel flow at very low Reynolds numbers. 2014, arXiv:1406.0248v2.

Micropolar Theory on Turbulence Modulation

George Sofiadis[1*], Evangelos Karvelas[2]
and Ioannis Sarris[2]
[1]Department of Mechanical Engineering, University of Thessaly, 38334, Volos, Greece
[2]Department of Mechanical Engineering, University of West Attica, Athens, Greece
* Corresponding Author: sofiadis@uth.gr*

Fluids with internal rigid microstructure, the so-called micropolar fluids, gain significant attention in many industrial, natural and biological systems. Typical examples of such fluids are dense suspensions, liquid crystals and blood flow. Here we study in detail their turbulent regime by considering an alternative formulation of the Navier-Stokes equation in which the linear and angular momentum is conserved for the fluid and its microstructure, respectively. Three cases of low-turbulence channel flow with Re = 3300, 5600 and 13800, based on mean velocity, channel height and the fluid kinematic viscosity are used to study the effect of polarity and Re.

Micropolar theory was originally developed by Eringen [1]. In his work, Eringen introduces a simple generalization of the usual Navier-Stokes equation system, the so-called micropolar equations, where due to internal fluid structure microrotation, an angular momentum conservation equation is also solved. In addition, new viscosity coefficients appear in the system of governing equations, as the main role of microrotation is to increase the dissipation of kinetic energy. These equations may be reduced to the classical Navier-Stokes equations when microrotation viscosity coefficients are diminished.

In the present study, Direct Numerical Simulations (DNS) of a turbulent channel flow with internal microstructure have been performed. The set of equations that has been solved (1) and (2), together with the incompressibility condition, $\nabla \cdot u = 0$, has been properly nondimensionalized as:

$$\frac{\partial u}{\partial t} + (u \cdot \nabla)u = -\nabla P + \frac{1}{Re}\nabla^2 u + \frac{m}{Re}\nabla \times \omega \qquad (1)$$

$$\frac{JN}{m}\left(\frac{\partial \omega}{\partial t} + (u \cdot \nabla)\omega\right) = \frac{1}{Re}\nabla^2 \omega + \frac{N}{Re}\nabla \times u - 2\frac{N}{Re}\omega \qquad (2)$$

where, u and ω are the linear and angular velocity, respectively, and P stands for pressure. Except of Reynolds number, the rest non-dimensional parameters are: $m = \kappa/(\mu+\kappa)$ the so-called vortex viscosity parameter where κ is the micropolar viscosity and μ the molecular one, $J = j/\delta^2$ the dimensionless microrotation based on δ^2, where j is the microinertia of the fluid, and $N = \kappa\delta^2/\gamma$ the so-called spin gradient viscosity parameter, where γ is the material coefficient of the fluid.

Three different Reynolds numbers are considered in the low Reynolds turbulent regime, while the ratio of micropolar to total viscosity *(m)*, has been varied as well, where micropolar viscosity is the one of the dispersed phase. Our findings support that turbulence behavior is affected by both *m* and *Re* [2]. Previous studies have also reported modulation of the turbulence activity in dilute suspensions, although the majority of these studies only considers the effect of particle diameter. They mostly report a turbulence attenuation when the particle diameter is less than the turbulent length scale. For low micropolar volume fractions, turbulence presents a monotonic enhancement as the Reynolds number increases. However, on the other hand, for sufficiently high-volume fractions, turbulence intensity drops, along with Reynolds number increment Fig. 1 [2]. This result is considered to be due to the effect of the micropolar force term on the flow, suppressing near-wall turbulence and enforcing turbulence activity to move further away from the wall.
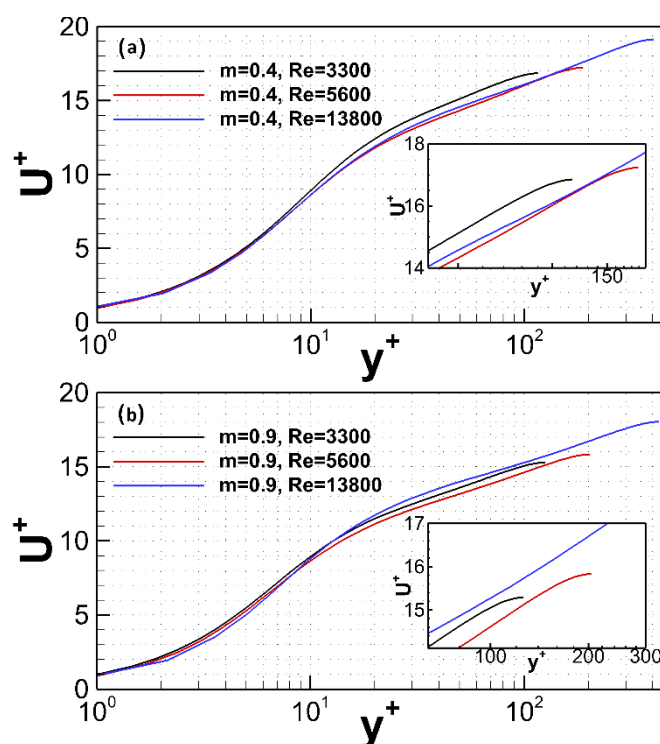
Fig. 1: Normalized mean streamwise velocity distributions along y+, for: m = 0.4, Re = 3300, 5600, 13800 and m = 0.9, Re = 3300, 5600, 13800 cases [2].

References

[1] Eringen, A.C. Theory of Micropolar Fluids; Technical Report; Purdue University: West Lafayette, Indiana, 1965; Volume 27.

[2] Sofiadis, G., and I. Sarris. Turbulence Intensity Modulation by Micropolar Fluids." Fluids 6, no. 6 (2021): 195.

Keynote Lecture

Oleg Goushcha

National Aeronautics and Space Administration (NASA), Langley, VA.
Adjunct Assistant Professor, Manhattan College, Riverdale, NY., USA

Oleg Goushcha combines his work at NASA with an Assistant Professorship in Mechanical Engineering. His research focuses on experimental fluid mechanics studying turbulent, transitional and vortical flows. Previous and current work include wind tunnel tests of passive-scalar mixing and energy harvesting in turbulent flows, fluid-structure interaction, and transition to turbulence and relaminarization in pulsating flows. His research is inspired by current needs in the clean technology and biomedical industries. Close interaction between academia and industry drives Dr. Goushcha to provide his students with theoretical tools and their practical applications in the industry.

Dr. Goushcha holds a B.S. and a M.S. in Aerospace Engineering, from the University of California, Irvine, and a Ph.D. in Mechanical Engineering, from The City College of New York. He has received several awards and grants from the City College of New York,

and

Yannis Andreopoulos

CUNY Distinguished Professor
Michael Pope Chair for Energy Research, Department of Mechanical Engineering
The Grove School of Engineering, The City College of New York, USA

Yannis Andreopoulos holds the Michael Pope Chair for Energy Research and is Professor of Mechanical Engineering at The Grove School of Engineering at The City College of New York. His research expertise is in the areas of fluid dynamics which impact transportation, manufacturing, medicine, biology, energy, the environment, built environment, climate change and defense and homeland security. Andreopoulos has developed several innovative experimental techniques and designed a large-scale wind tunnel and a unique high energy/enthalpy experimental shock tube research facility for studies in various configurations where high spatial and temporal resolution is required.

Andreopoulos holds an Engineering Diploma (Dipl.-Ing) in Mechanical and Electrical Engineering from the National Technical University in Athens, Greece, a M.Sc. (Aeronautics) from London University in England, a Diploma of Imperial College degree (D.I.C) and a PhD in aeronautical engineering from Imperial College of Science, Technology and Medicine of London University, UK. He held postdoctoral research appointments at the University of Karlsruhe, Germany, and at Princeton University where he gained extensive experience in laser techniques and optical methods.

Yannis Andreopoulos has been unanimously elevated by the CUNY Board of Trustees, to the rank of Distinguished Professor, the highest academic honor that CUNY can bestow upon faculty who have reached exceptional scholarly achievement.

Lecture title:
Vortices interacting with smart materials and structures: the case of energy harvesting
by Oleg Goushcha, Vahid Azadeh Ranjbar, Yiannis Andreopoulos

The lack of understanding and the complexity of vortex induced vibration (VIV) physics combined with a diverse range of applications have motivated a number of studies in this field. While large vibration amplitude due to VIV in general should be avoided in the design of engineering systems since the induced deflections can cause significant structural stresses, new applications related to harnessing small-scale energy from the ambient environment using VIV have emerged in the last decade which have revived the interest in this field. Recent advances in decreasing the power consumption of electronic devices, such as remote sensors, have bolstered the interest in clean and renewable energy harvesting. Converting ambient mechanical vibration to electrical power by using electromechanically coupled smart materials has been the main focus of the present energy-harvesting research. In the last several years, research has concentrated on harvesting energy from fluid flows, which otherwise is wasted, by using vibrating structures, mostly cantilever beams with piezoelectric layers, which are excited by fluid-structure interaction. The presentation will include configurations that can be classified as interactions with forcing stimuli provided by coherent fluid structures such as vortices with distinct travel frequency and spacing, like those in the wake of cylinders, discrete vortex rings, or randomly appearing turbulent eddies in boundary layers or grid turbulence. The excited motion of the structure with the piezoelectric transduction can lead to simple vibrations by flutter or complex VIV.

Keynote Lecture

Xiande Fang
Distinguished Professor
Nanjing University of Aeronautics and Astronautics (NUAA), China

Xiande Fang is a distinguished professor at Nanjing University of Aeronautics and Astronautics (NUAA), China. He received his Ph.D. in Engineering Thermophysics from University of Science and Technology of China, M. Sci. in Thermal Engineering from Tsinghua University, China, and B. Eng. in Altitude Equipment from NUAA. He is currently an Associate Editor, Aerospace Science and Technology (SCI indexed top journal), and the Editor-in-Chief, International Journal of Thermofluid Science and Technology. He worked as an associate researcher in USA for one year, and as a visiting professor and professional engineer in Canada over 5 years. In NUAA, he serves as the deputy director of Academic Committee of MIIT Key Laboratory of Aircraft Environment Control and Life Support and the director of Professional Committee of Building Environment and Energy Engineering and Aircraft Environment Control and Life Support Engineering. His research area is thermofluid science and technology and its applications to various industrial sectors. He has published over 200 papers and 4 books/book chapters, received 14 academic awards, and obtained 15 Chinese patents. He teaches thermofluid-related courses to international undergraduate, postgraduate, and doctoral students in China.

Lecture title:
Empirical Predictive Method for Two-Phase Flow Condensation Heat Transfer in Plain Channels

Empirical Predictive Method for Two-Phase Flow Condensation Heat Transfer in Plain Channels

Xiande Fang[*], **Xiaohuan Li, Zufen Luo, Gen Li**

Key Laboratory of Aircraft Environment Control and Life Support, MIIT, Nanjing University of Aeronautics and Astronautics, 29 Yudao Street, Nanjing, PR China
* Xiande Fang: xd_fang@nuaa.edu.cn

The heat transfer (HT) of gas-liquid two-phase flow condensation in plain channels is widely used in many industrial sectors, and thus it is important to predict accurately the heat transfer coefficient (HTC). The recent evaluations of correlations for flow condensation HTCs with large databases showed that there was still a considerable room left for improving the prediction accuracy [1]. Flow condensation HTCs are affected by various parameters, making it a challenge for decades to develop an accurate correlation with a wide application range. The present study presents a new correlation with high accuracy in wide parameter range for predicting flow condensation HTC in plain channels.

The experimental studies of flow condensation HT in plain channels were reviewed. A database containing 5591 experimental data points of flow condensation HTCs were compiled from 33 data sources, covering 27 fluids and wide parameter ranges.

Based on the database, 32 existing HTC correlations of flow condensation HT in plain channels were evaluated and analyzed to find clues for developing a new correlation.

A new HTC correlation of flow condensation with high accuracy is developed based on the database and a systematic methodology. It is of the form

$We_{go} \leq 500$

$$Nu = \begin{cases} 0.915\left(Gr^{0.22} + \left|Gr^{0.65} - 1\times10^4\right|^{0.28}\right)Pr_l^{0.25} Pr_g^{-0.7} Fa^{-0.2} \\ \quad \left(\dfrac{x}{1-x}\right)^{0.25}\left(\dfrac{\mu_l}{\mu_g}\right)^{-0.1} \qquad\qquad Gr < 4\times10^6 \\[2ex] 1.49 Gr^{0.45} Pr_l^{0.3} Re_{lo}^{-0.6} Pr_g^{-0.4} Fa^{-0.25}\left(\dfrac{x}{1-x}\right)^{0.2}\left(\dfrac{\mu_l}{\mu_g}\right)^{0.25} \\ \qquad\qquad\qquad\qquad 4\times10^6 \leq Gr < 1.5\times10^8 \\[2ex] 21.2 Gr^{0.12} Pr_g^{-0.4}\left(\dfrac{x}{1-x}\right)^{0.15} \qquad Gr \geq 1.5\times10^8 \end{cases}$$

$We_{go} > 500$

$$Nu = \begin{cases} 0.00126(1-x)^{-0.1}\left(Gr^{0.2} + \left|Gr - 2\times10^6\right|^{0.24}\right)(Re_g + 0.43Re_l)^{0.5} \\ \quad Pr_l^{0.35} Fa^{0.1} We_{go}^{0.33} \qquad\qquad Gr < 4\times10^6 \\[2ex] 1.03\left(Gr - 2\times10^6\right)^{0.05} Re_g^{0.45} We_{go}^{0.3} \quad 4\times10^6 \leq Gr < 1.5\times10^8 \\[2ex] 0.00353\left(Re_g + 5\times10^4\right)^{0.75} We_{go}^{0.33} Fr_{lo}^{-0.2} \qquad Gr \geq 1.5\times10^8 \end{cases}$$

$$(1)$$

where x is the quality, μ is the dynamic viscosity, subscripts l, lo, g, go, denote liquid, liquid only, gas, and gas only, respectively, and the dimensionless parameters are explained in Table 1.

Table 1: Dimensionless parameters in Eq. (1)

Dimensionless number	definition
Fang number	$Fa = (\rho_l - \rho_g)\sigma/(G^2 D)$
liquid only Froude number	$Fr_{lo} = G^2/(gD\rho_l^2)$
Grashof number	$Gr = g\rho_l(\rho_l - \rho_g)D^3/\mu_l^2$
Prandtl number	$Pr_k = c_{pk}\mu_k/\lambda_k$
liquid Reynolds number	$Re_l = (1-x)GD/\mu_l$
gas Reynolds number	$Re_g = xGD/\mu_g$
liquid only Reynolds number	$Re_{ko} = GD/\mu_k$
liquid only Weber number	$We_{ko} = G^2 D/(\rho_k\sigma)$

where c_p is the constant pressure specific heat, ρ is the density, g is the gravity, λ is the thermal conductivity, σ is the surface tension, D is the channel diameter, and subscript $k = l$ denoting liquid and $k = g$ denoting gas.

The steps for developing the new correlation is summarized below:

(1) Determining the candidate dimensionless parameters that are possibly incorporated into the new correlation.

(2) Constructing tentative model forms and determining baseline model forms.

(3) Modifying the baseline model forms using the least squares and error analysis along with adding/removing some dimensionless parameters.

(4) Steps (2) and (3) are repeated until the satisfactory result is obtained.

The new correlation improves the prediction accuracy remarkably, having a mean absolute deviation (MAD) of 14.9% for the entire database, as shown in Table 2, much better than the best existing one having an MAD of 17.1%.

$$\text{MAD} = \frac{1}{N}\sum_{i=1}^{N}\left|\frac{y(i)_{pred} - y(i)_{exp}}{y(i)_{exp}}\right| \qquad (2)$$

where subscripts *pred* and *exp* are the predicted and the measured values, and N is the number of the total data points.

Table 2: MADs of the new and the best existing correlations (%)

Correlation	Total data	$D \geq 3$ mm	$D < 3$ mm
New	14.9	14.8	15.0
Cavallini et al. [2]	17.1	16.1	19.6

References

[1] Shah MM. A correlation for heat transfer during condensation in horizontal mini/micro channels. Int. J. Refrigeration, 2016, 64: 187–202.

[2] Cavallini A, Del Col D, Doretti L, Matkovic M, Rossetto L., Zilio C, Censi G. Condensation in horizontal smooth tubes: a new heat transfer model for heat exchanger design, Heat Transfer Engineering, 2006, 27(8): 31–38.

Keynote Lecture

Toshihiko Shakouchi
Professor, Emeritus
Graduate School of Engineering
Mie University, Japan

B.S. Eng., 1969 and M.S. Eng., 1971, Ehime University, and Dr. Eng., 1984, Nagoya University, Japan
Guest researcher, 1992-1993, Erlangen-Nuremberg University, Germany.
Chairperson of *The 1st Int.Conf,on Jets, Wakes and Separated Flows, ICJWSF-2005*, 2005, Toba-shi, Japan.
President of *Japan Soc. for Multiphase Flow, JSMF*, 2009.
Fellow of *Japan Soc. of Mechanical Engineers, JSME.*
Emeritus member of *JSMF.*
Interests
- Jets, wakes and separated flows
- Coanda reattached jet, Resonance jet, Oscillating jet, Edge-tone
- Supersonic Jet; Vector control, Gas atomization, Ejector
- Flow control
- Fluidics
- Gas-solid flow; Air classification of fine solid particles, Jet mill, Blaster
- Gas-liquid flow; Drag reduction, Gas absorption, Jet oscillation, FAC
- Heat transfer; Impinging jet, Oscillating jet, Heat exchanger
- Desalination of sea water by decompressed boiling

Lecture title:
Flow and Control of Some Jets and Separated Flows

One of the major purposes of fluid mechanics and engineering is to reduce the flow resistance caused by flow friction, flow separation, vortex generation, and others. To reduce the flow resistance, in general, flow control is carried out by a passive or an active method in order to reduce or increase the flow resistance depending on the needs. Passive flow control is performed by changing the configuration of flow channel or object a little and reducing the total flow resistance. On the other hand, active flow control uses a device requiring power, but it can perform various complex flow controls. In this lecture, the passive flow control of jets and separated flows is examined with flow characteristics, control methods, and some applications because jets and separated flows include the essence of fluid dynamics, such as, boundary layer flow, turbulent flow, shear flow, vortex flow and flow mixing. In particular, the effects of the nozzle shape, the tab, rib and vortex generator, and the orifice or notched orifice on the flow characteristics of sub- and supersonic jets are examined. Furthermore, the control and suppression of high speed jet noise by a chevron nozzle, some examples of active flow control, and other areas are examined. Globular formation of fine solid particles by flow control, lift control of airplane wings, and the flow control of a NOTAR helicopter without tail rotor are also addressed.

Experimental study on the heat transfer characteristics and frequency control of flashing spray cooling under varying operating conditions

Shang-Ming Wang, Zhi-Fu Zhou, Bin Chen*

State Key Laboratory of Multiphase Flow in Power Engineering, Xi'an Jiaotong University, Xi'an 710049, China
* Corresponding Author: chenbin@mail.xjtu.edu.cn

As electronic chips tend to become more and more compact, traditional cooling methods can hardly satisfy the requirement of extremely high power density and low working temperature. With high heat transfer coefficient and critical heat flux (CHF) at low surface temperature, flashing spray cooling is considered as one of the most promising thermal management technologies, and its in-depth research has far-reaching significance for the optoelectronic manufacturing industry[1].

In this work, a close loop experimental rig was constructed to study the heat transfer characteristics of flashing spray cooling by R410A in steady-state, varying operating conditions and the frequency conversion, especially the effects of compressor frequency conversion on system parameters including mass flow rate, chamber outlet pressure, time required to reach steady state, and system cooling performance. The experimental system consists of an inverter compressor, a condenser, a spray chamber and a liquid-vapor separator and other accessories. The discharge pressure of the compressor can be up to 4.1 MPa. As shown in Fig. 1, the spray chamber is made of stainless steel high-pressure resistant cavity with tempered glass window. A nozzle with inner diameter of 0.8 mm sprays R410A droplets onto the smooth flat copper cooling surface. The distance between nozzle orifice and the cooling surface is 24.5 mm. To simulate chip heating, the bottom of the cooling surface is supported by a copper heating body, which is embedded with 10 evenly distributed heating rods and the heating power is changed by a voltage regulator. Two probe type K-type thermocouples are embedded at 9mm and 13.8mm below the cooling surface, and the recorded temperature is used to obtain the heat flux of the cooling surface by Fourier heat conduction.
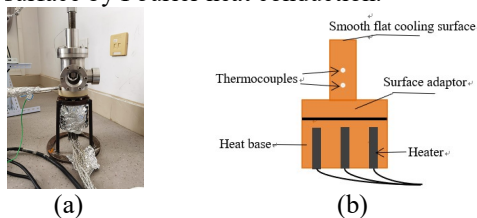
(a)   (b)
Fig. 1: Spray chamber (a) and test section (b)

The experimental results show that system takes 1200-1800s to reach the steady state. With increasing the heating voltage, phase change of the refrigerant inside the chamber can be observed. The heat transfer process of flashing spray cooling will experience three stages: single-phase heat transfer, two-phase boiling and partial drying, In the stage II, the heat transfer effect and cooling performance of the spray cooling system are the best. With increasing the compressor frequency, the mass flow rate of refrigerant in the system increases. The outlet pressure of the

spray chamber has a linear negative correlation with frequency, and it is less influenced by the heat flux. In addition, an increase in compressor frequency can shorten the time consumed for the system to reach steady state.

From the Fig. 2 and Fig. 3 we can analyze the cooling performance of the system for different compressor frequency. When the compressor frequency is 10Hz, 15Hz and 20Hz, for smooth flat surface, CHF can reach 162.89 $W \cdot cm^{-2}$, 168.31 $W \cdot cm^{-2}$ and 175.02 $W \cdot cm^{-2}$, separately, at the condensation temperature of 26℃. In the heat transfer stage II with good heat transfer effect, the heat transfer coefficient falls within the interval [53.71, 72.28], [64.15, 88.62], [72.64, 99.94] $kW \cdot m^{-2} \cdot k^{-1}$, respectively. Meanwhile, the temperature of the chip surface can be maintained below 35℃, 30℃ and 25℃ in this stage. It is shown that the increase of compressor frequency can effectively improve the refrigeration performance of the whole system.
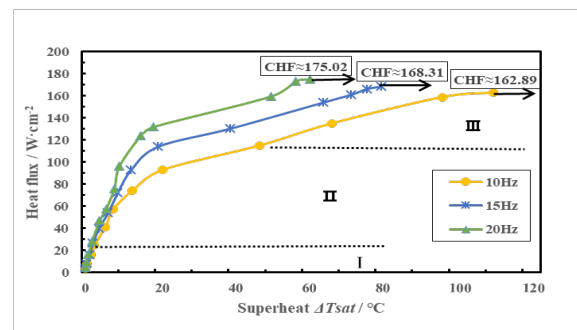
Fig. 2: Heat flux as a function of surface superheat for different compressor frequencies
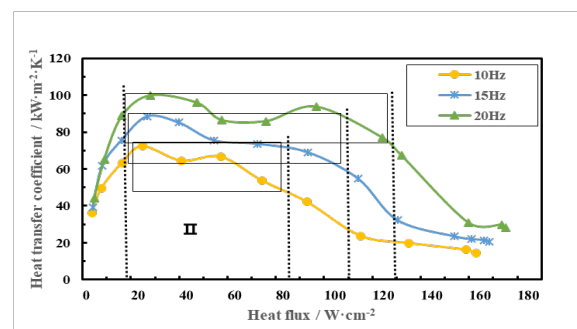
Fig. 3: Heat transfer coefficient as a function of heat flux for different compressor frequencies

References

[1] Bostanci Huseyin and Yata Vishnu V. R. and Kaluvan Suresh. Flow-Controlled Spray Cooling Approaches for Dynamic Thermal Management[J]. Journal of Electronic Packaging, 2021, 143(3):1-8.

Influence of the inlet local annular swirling zone on an axisymmetric turbulent jet

Yevhenii Shkvar[1]*, Shi-ju E[1], Dmytro Redchyts[2], Svitlana Moiseienko[3]

[1]College of Engineering, Zhejiang Normal University,688 Yingbin Road, Jinhua, Zhejiang Province, 321004, China
[2]Institute of Transport Systems and Technologies of the NASU, Pysarzhevskoho str., 5, Dnipro, 49005, Ukraine
[3]Kherson National Technical University, Beryslavske highway, 24, Kherson, 73008, Ukraine
* Corresponding author: shkvar.eugene@qq.com

Vortex formation is an effective mechanism for modifying the structure of various flows, capable of enhancing mixing and affecting the distribution of characteristics of turbulence, heat and mass transfer. There are many designs of efficient nozzles that form swirling jets, which are effectively applied in various engineering devices and, in particular, for the preparation and injection of droplet-air fuel mixtures into the combustion chambers of various engines [1]. The object of this research is the high-temperature ($t \leq 650°C$) axisymmetric free turbulent jet ($U \leq 30$ m/s), in which a swirl is generated only for some inlet annular zone using a special impeller with blades, installed on the core part of exit section of the air-heating element (Fig. 1). Such kind of flow can be formed, for example, by the typical heat-gun device, but its area of possible implementations is much wider. The main goal is to analyze the influence of a local swirl effect of the internal annular part of flow on the velocity and temperature distributions in axial x, radial r and angular φ directions for the flow regions, located both inside and outside the nozzle.
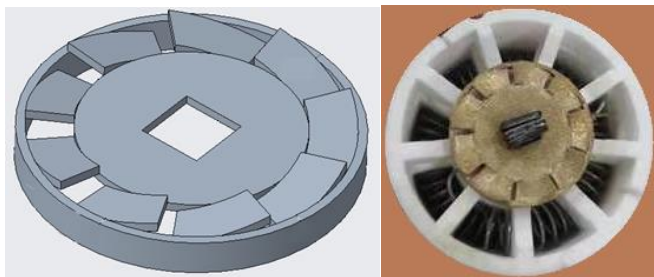
Fig. 1: Impeller for creating the local annular swirling flow

The principal idea is the creation of the tangential velocity component 2 by the blades of deflector 1, which locally swirls the flow (Fig. 2). An important aspect of the studied innovation is the effective use of the interaction between the swirling component of the flow from the blades 3 of the impeller 1 and the disk deflector 4 installed inside the nozzle 5 to increase the jet speed at its exit section.
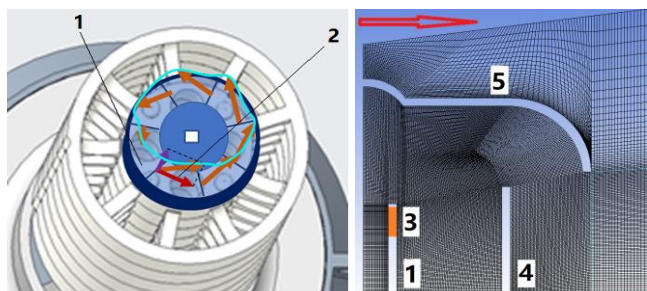
Fig. 2: Principal structure of the proposed swirl nozzle and the applied structured mesh for numerical flow modeling

The studies have been performed both theoretically (RANS & k-ω SST modeling) and experimentally (Pitot-Darcy & TR-PIV measurements). The numerical predictions, obtained using the developed numerical model, correlate qualitatively with the corresponding experimental data for the analyzed flow, and the quantitative discrepancies do not exceed 15%. The detailed flow structure (Fig. 3) allows to conclude about beneficial realization of the effect of the angular velocity intensification in the inner part of the free jet due to the flow turn on the edge of the deflector 4 and in accordance with the 2-nd Helmholtz's theorem.
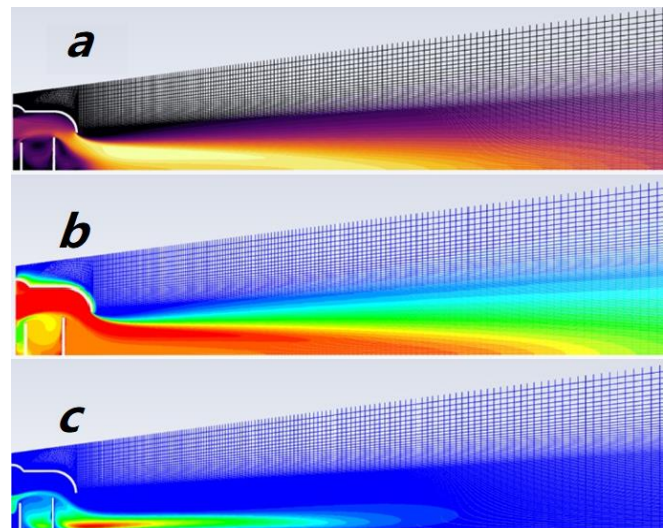
Fig. 3: Numerical prediction of the jet parameters: *a* – velocity magnitude $U(x,r)$; *b* – temperature distribution $t(x,r)$; *c* – swirl velocity $W(x,r)$

Conclusions. The realized swirl effect allowed to achieve a uniform flow structure in the angular direction even with sufficiently strong inhomogeneities of the flow at the inlet, which have different technological reasons. At the same time, the proposed implementation of the local annular flow swirl is quite efficient and rational from the point of view of additional energy losses, associated with its implementation. Further improvement of the proposed technology can be aimed at optimizing the size, placement and intensity of swirling of the annular vortex-forming region 3 of the inner impeller 1.

References

[1] Vasilyev A. Yu., Sviridenkov A. A., Tretyakov V. V. Experimental investigations of fluid atomization by model frontal devices of combustion chambers [J] Samara State Aerospace University Bulletin, 2011, 5 (29):55-64.

Experimental Study on Coaxial Swirling Jets

A. Naxakis, A. Romeos, A. Giannadakis, K. Perrakis, Th. Panidis*

Department of Mechanical Engineering & Aeronautics, University of Patras
Rion-Patras, 26504, Greece
* Corresponding Author: panidis@upatras.gr

Experimental results on coaxial swirling flows are presented, aiming to contribute to the investigation and understanding of vortical flows close to vortex breakdown conditions[1-5]. Two swirling streams are issuing from parallel coaxial straight tubes in a coaxial cylinder of diameter equal to the largest tube. Swirl is introduced by two rotating vanes located close to the outlets of both jets respectively (fig 1). Initial conditions, flow rates and swirling strengths can be parametrically controlled, for both streams. The mean flow field is monitored on the axial central plane, based on measurements of all three velocity components, using Stereoscopic PIV. In the present experiments three inner and six annular flow rates were combined with four inner jet and three annular jet swirls comprising a relatively large number of inlet conditions.
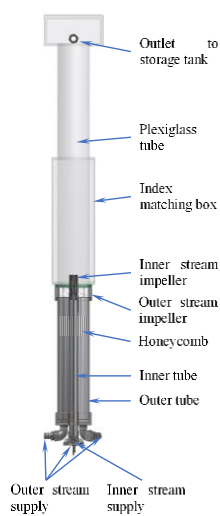
Fig. 1: Experimental Setup

The difference between the internal and external mean longitudinal velocities was considered to represent the linear momentum affecting the flow field, while the co-rotating angular velocities were expected to have an additional effect on the angular momentum and their ratio was used as a reference Rossby number, Ro_{tot}.

$$Ro_{tot} = \frac{V_{y,i} - V_{y,o}}{V_{\theta,i} + V_{\theta,o}} \qquad (1)$$

The use of the modified Rossby number was not sufficient to unambiguously describe the observed trends and determine the flow types. An additional dimensionless number S_2 was devised to support the identification of flow types in relation to the input conditions.

$$S_2 = \frac{V_{\theta,i}}{V_{y,i}} \frac{(V_{y,i} - V_{y,o})}{(V_{\theta,i} - V_{\theta,o})} \qquad (4)$$

Based on the combination of Ro_{tot} and S_2, an experimental map of flow conditions has been constructed, to classify the flow patterns (fig 2). Four typical flow patterns can be identified for different inlet conditions. A "downstream core flow" (DCF) in test cases with no recirculation, a "closed bubble" type (CB) vortex breakdown, an "asymmetric recirculation" (AR) and an "intense recirculation" (IR) pattern.
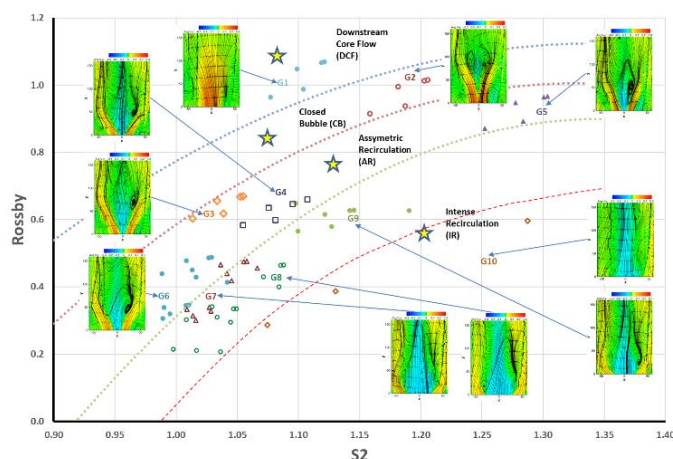
Fig. 2: Flow map in accordance with Ro_{tot} and S_2

References

[1] Escudier, M. (1988). Vortex breakdown: observations and explanations. Progress in Aerospace Sciences, 25(2), 189-229.

[2] Champagne F. H., Kromat S., Experiments on the formation of a recirculation zone in swirling coaxial jets, Experiments in Fluids, 2000, Volume 29, Issue 5, pp 494–504

[3] Ivanic, T., Foucault, E., & Pecheux, J. (2003). Dynamics of swirling jet flows. Experiments in fluids, 35(4), 317-324.

[4] Giannadakis, A., Perrakis, K., & Panidis, T. (2008). A swirling jet under the influence of a coaxial flow. Experimental Thermal and Fluid Science, 32(8), 1548-1563.

[5] Naxakis A., Perrakis K., Panidis T. (2018). Experimental study on swirling jets. International Review of Mechanical Engineering, 12(6), 533-539.

Patient–Specific Diastolic Vortex Flow Patterns in the Left Ventricle

Dimitris Zantzas[1*], Vasileios G. Gkoutzamanis[1] Vasiliki Kantartzi[2] Vasileios Sachpekidis[2] and Anestis Kalfas[1]

[1]*Aristotle University of Thessaloniki, School of Mechanical Engineering, GR-54124 Thessaloniki, Greece,*
[2]*Papageorgiou General Hospital 2nd Cardiology Department, GR-56429 Thessaloniki, Greece*
* Corresponding Author: dzantzas@auth.gr

This paper presents a numerical model for the analysis of blood flow in a human left ventricle during the diastolic phase. Patient–specific data from Real-Time 3-Dimensional Echocardiography is used in order to reconstruct the geometry of left ventricle. Vortex flow pattern analysis is conducted in order to quantify the role of vortical structures in the optimal throughput of the heart flow.

In order to broaden our knowledge about the heart function and to counter the increasing cardiovascular diseases novel approaches are required. Computational engineering could be very productive for this purpose. The vortex formation in the left ventricle is suggested to critically contribute to efficient blood pump function[1]. For that reason, this paper is focused on the qualitative analysis of the role of the vortex that appears in the left ventricle.

In this paper, the geometry of the model is reconstructed from patient-specific data. The segmentation process is made manually with the use of semi-automatic algorithms. The temporal resolution of the echo data is too low for the numerical simulation, so cubic splines interpolation is used to fit the requirement of the CFD calculation with the reconstructed geometries[2]. The calculation is performed using a Navier-Stokes solver with the use of the arbitrary Lagrangian Eulerian formulation. The working fluid simulating blood is taken to be a Newtonian fluid with constant viscosity and density.[3]

Analysis of the results shows that the velocity and the pressure inside the left ventricle are in reasonable agreement with in-vivo data which have been acquired by clinicians. In figure 1 and 2, cross-sectional view of the blood pressure and the 3D vortex ring with velocity vector is presented in two consecutive timesteps of the diastolic phase. The vortex ring is considered to assist ventricular function[4].
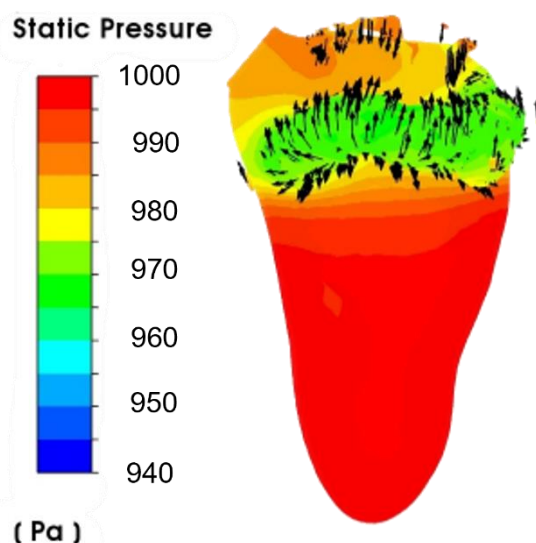
Fig. 1: Static pressure and 3D vortex at early diastole.
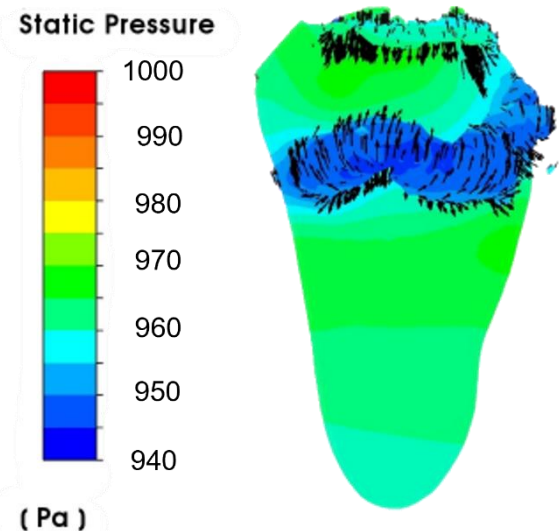
Fig. 2: Static pressure and 3d vortex at mid-diastole.

This vortical motion has been found to occur in the early diastolic phase as shown in figure 1. Furthermore, this vortical motion is found to persist almost the whole diastolic phase of the cardiac cycle. As depicted from the two figures, the 3D vortex ring is found in the region of minimum pressure and is migrated to the apex with the evolution of diastolic phase.

References

[1] Gharib, Morteza & Rambod, Edmond & Kheradvar, Arash & Sahn, David & Dabiri, John. (2006). Optimal vortex formation as an index of cardiac health. Proceedings of the National Academy of Sciences of the United States of America. 103. 6305-8. 10.1073/pnas.0600520103.

[2] Schenkel T, Malve M, Reik M, Markl M, Jung B, Oertel H: MRI-based CFD analysis of flow in a human left ventricle: methodology and application to a healthy heart. Ann Biomed Eng. 2009, 37: 503-15. 10.1007/s10439-008-9627-4.

[3] Khalafvand, Seyed Saeid & Zhong, Liang & Ng, Eddie. (2014). Three-dimensional CFD/MRI modeling reveals that ventricular surgical restoration improves ventricular function by modifying intraventricular blood flow. International Journal for Numerical Methods in Biomedical Engineering. 30. 10.1002/cnm.2643.

[4] Krueger PS, Gharib M: The significance of vortex ring formation to the impulse and thrust of a starting jet. Phys Fluids 15:1271-1281, 2003

Hot-wire measurement of asymptotic characteristics of lobed jet flow

Ren Fukui[1*], Mamoru Takahashi[1], Koichi Tsujimoto[1],
Toshitake Ando[1], Toshihiko Shakouchi[1], Ryuichi Momiyama[2]

[1] *Graduate school of Engineering, Mie University, Tsu, Mie, Japan*
[2] *Faculty of Engineering, Mie University, Tsu, Mie, Japan*
Corresponding Author: 421M49@m.mie-u.ac.jp

1. Introduction

Diffusion characteristics of the turbulent jet can be controlled by modifying the initial condition, namely the nozzle shapes. Lobed jet is one of the non-circular jets, supplied from the nozzle with a wave-shaped edge. Originally this idea is from the noise reduction of the jet engine but has potential for more applications in mixing enhancement problems.

Nastase et al. [1] investigated the lobed jets with six lobes. They found better mixing efficiency of the lobed jets than the round one in the near-field. However, they showed the results obtained only in x≲$10D_e$, where x is the streamwise distance from the nozzle exit and D_e is the equivalent diameter of the jet exit. In order to understand the whole area of the jet flow field, measurement of the asymptotic (self-similarity) characteristics of the jet is desired. Wygnanski et al. [2] showed that the half-width of the mean velocity of the turbulent wake depends on the initial condition, even though that of the mean velocity profile itself does not. This suggests that the lobed jets have different diffusion characteristics from the round jet.

In the present study, we investigated the asymptotic diffusion characteristics of two lobed jets which have six lobes. The results were compared with that of the round jet.

2. Experimental setup

The jet flows are generated in the laboratory experiment. The air flow was supplied by a blower, and cooled by a radiator, before being ejected from the nozzle of a wind tunnel into the still air. The flow rate was monitored by a digital manometer connected to a flowmeter, and we adjust the flow rate with the valve installed between the radiator and the flowmeter. The jet flows were measured by a hot-wire anemometer with I-type probe. The hot-wire sensor was a tungsten wire of 5 μm in diameter and 1 mm in length. Figure 1 shows the edge shapes of the round and lobed nozzles. The shapes of the lobed nozzles are given by

$$r(\theta) = D_e\sqrt{\frac{2b^2}{2b^2+1}}\left(1 + \frac{\cos a\theta}{b}\right) \ , \qquad (1)$$

where the parameter a and b are the number of lobes and curvature of the edge, respectively. In the present study, we used a=6 and b=2 or 4. The (equivalent) diameter of the nozzles were 15 mm. The nozzles can form the top-hat initial mean velocity profiles, which is generally achieved by a smooth contraction nozzle.

Reynolds number Re≡$D_e U_J/v$ is 70,000, where U_J is the mean velocity at the jet exit (≃70 m/s) and v is the kinematic viscosity of the air (≃1.5×10⁻⁵ m²/s). 524,288 instantaneous samples are obtained with 20 kHz sampling frequency.
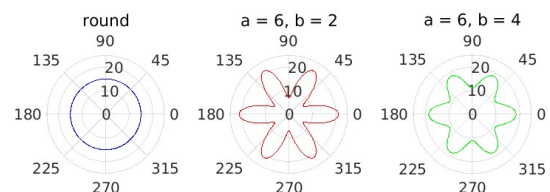
Fig. 1: Shape of the nozzles
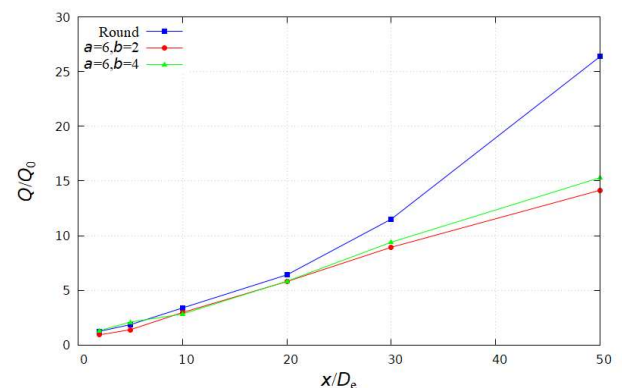
Fig. 2: Development of the normalized flow rate

3. Results

Figure 2 shows the development of the flow rate of the round and lobed jets. The flow rate is normalized using that at the nozzle exit (Q_0) and the distance x using D_e. The flow rate was obtained by integrating the mean velocity over the cross-streamwise plane at each measurement distance, but the small value at the outer edge of the jet (less than 10% of the value at the jet centerline). It can be observed that the flow rate of the lobed jets is smaller than that of the round jet in the far-field. In contrast, there was no difference in the lobed jets with different curvatures.

4. Conclusions

- The flow rate of the lobed jet is smaller than that of the round jet in the far field.
- The asymptotic diffusion characteristics of the lobed jets are independent of the curvature of the nozzle edge.

References

[1] Nastase I, Meslem A. Vortex dynamics and mass entrainment in turbulent lobed jet with and without lobe deflection angles. Experiments in Fluids, 2010, 48(4):693-714.

[2] Wygnanski I, et al. One the large-scale structures in two-dimensional, small-deficit, turbulent wakes. Journal of Fluid Mechanics, 1986, 168:31-71.

Vortex Structure Produced by a Sweeping Jet in a Cross Flow

Masaki Fuchiwaki[1*], Eisei Kobayashi[1], Surya Raghu [2]

[1] *Kyushu Institute of Technology, Kawazu6804, Iizuka, Japan*
[2] *Advanced Fluidics LLC, 8860 Columbia 100 Parkway, Suite 204, Columbia, MD 21045, USA*
* *Corresponding Author:futiwaki@mse.kyutech.ac.jp*

Fluidic Oscillator generates a sweeping jet with high frequency and large amplitude and is characterized by its capability for jet ejection over a wide range. Recently, the sweeping jet from the Fluidic Oscillator has been attracted attention from the viewpoint of an active flow control techniques. The studies on the active flow control techniques using the sweeping jet have been already reported [1]-[3]. However, these studies focused on the characteristics of the dynamic forces acting on an airfoil in conjunction with a fluidic oscillator. There have been no studies about the flow structure or flow mechanism. Actually, the sweeping jet from the Fluidic Oscillator ejected into a main flow is the jet in cross flow, and it is well known that this flow field will be more complex flow structure. It is expected that the interaction between the sweeping jet and the main flow occurs and the complex vortex structure will be generated in the wake. In near future, in order to apply as the active flow control devise using the sweeping jet from the Fluidic Oscillator, it is required to be understood the complex flow structure and the flow mechanism by the interaction between the sweeping jet and the main flow.

The authors have already reported the flow characteristic produced by interactions between the sweeping jet from the fluidic oscillator and the main flow using a stereo particle image velocimetry (PIV) measurement [4]. However, the detailed of the flow structure or flow mechanism produced by the interaction between the sweeping jet and the main flow have not been understood sufficiently.

The purpose of the present study is to investigate the detailed vortex structure produced by the interaction between the sweeping jet from the Fluidic Oscillator and the main flow. Especially, the detailed vortex structure and flow mechanism produced by these interactions is visualized by a stereo PIV measurement and a numerical simulation using ANSYS-CFX.

The three-dimensional velocity vectors in x-y plane produced by the interaction between the sweeping jet and the main flow at a location 30 mm from the outlet of the jet obtained by the stereo PIV is shown in Figure 1(a) and 1(b). Figures 1(a) and 1(b) shows the results at $V_j/V_0 = \infty$ ($Vo = 0.0$ m/s) and 80.00, respectively. These results are time-averaged results during 0.5 sec. At $V_j/V_0 = \infty$, as shown in Fig. 1(a), the sweeping jet from the fluidic oscillator shows high-speed flow to the right and left. All velocity vectors are linear and the rotational component of the velocity field is not seen. On the other hand, at $V_j/V_0 = 80.0$, as shown in Fig. 1(b), the high-speed jet is especially prominent in the center and the maximum velocity of the sweeping jet is much higher than that at $V_j/V_0 = \infty$. The higher velocity vectors at the center of the sweeping jet are surrounded by the low velocity vectors with a strong rotational component at the outside of the

sweeping jet. It is expected that the low velocity vectors with a strong rotational component at the outside is produced by the interaction between the sweeping jet and the main flow and the higher velocity at the center is induced by the interaction. Moreover, the spreading angle of the sweeping jet is greater than at $V_j/V_0 = \infty$. The PIV measurement results will be related with the numerical simulation results, and finally, the authors will discuss about the more details of flow structure and the flow mechanism by the interaction between the sweeping jet and the main flow

(a) $V_j/V_0 = \infty$

(b) $V_j/V_0 = 80.0$
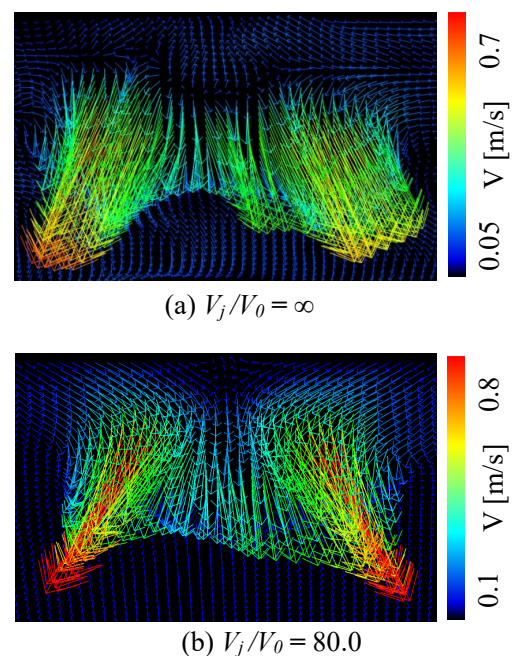
Fig. 1: Three-dimensional velocity vectors in x-y plane produced by the interaction between the sweeping jet and the main flow

References

[1] Raghu, S., Raman, and G., Miniature fluidic devices for flow control, *ASME-JSME joint fluids engineering conference*, 1999, ASME FEDSM 99-7256.

[2] Raghu, S., Gregory, J., W., and Sullivan, J., P., Modulated high frequency fluidic actuators for flow control, 2005, *International conference on jets, wakes and separated flows*.

[3] Raghu S., Fluidic Oscillator for flow control, 2013, *Experiments in Fluids*, 54:1455, DOI 10.1007/s00348-012-1455-5.

[4] Fuchiwaki, M., and Raghu S., Flow structure formed by a sweeping jet ejected into a main flow, 2018, *ASME 2018 5th Joint US-European Fluids Engineering Summer Conference,* FEDSM2018-83045

Supersonic Under-Expanded Reattached Jet with Vortex Region

Tetsuji Ohmura[1,2], Toshihiko Shakouchi[1*], Ryota Matsui[1] and Koichi Tsujimoto[1]

[1]*Mie University, Kurimamachiya-cho 1577, Tsu-shi, Japan*
[2]*Fukuda Metal Foil & Powder Co., Ltd., Kyoto, Japan*
* Corresponding Author: shako@mach.mie-u.ac.jp

If there is a wall near the incompressible jet, it reattaches to the wall surface by the Coanda effect enclosing a large vortex region (Fig. 1) [1]. The supersonic jet also reattaches to he wall, however the flow characteristics of supersonic reattached jet have not been revealed enough. The reattached jet is one of the basic flow in the fields of fluid- and thermo-dynamics. In this study, the flow characteristics such as the velocity, pressure, density distributions and the effects of offset distance on the two-dimensional supersonic under-expanded reattached jet are examined by numerical and experimental analyses.

Figures 1(a),(b) show, respectively, the velocity and pressure distributions by a 2-D numerical analysis using CFD software of the FlowSimulation with k-ε turbulence model. The supply pressure is $P_0 = 0.4$ MPa and offset distance is $D/b = 5.0$ (b: nozzle width = 2.5 mm, Aspect ratio: **4.0). Read colored area is a high speed area. The under-**expanded jet spreads just after the nozzle exit and appears the expansion region with a high speed and the compression region. This is the so called 1st shock cell. The 1st to 5th shock cells can be seen. The expansion and compression regions have negative low and positive high pressure areas (Fig. 1(b)). The dark blue and red colored areas in Fig. 1(b), respectively, are them. The jet reattaches to the side wall by the Coanda effect and there are major vortex region of clockwise and minor vortex region of counterclockwise near

Fig. 2: Pressure distribution on side wall
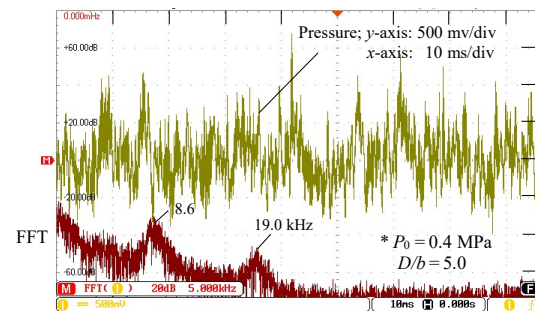
Fig. 3: Pressure fluctuation near reattachment point

the corner. However, the pressure distribution in the major vortex region is different from the incompressible reattached jet [1] and it does not have a cleat vortex center. Figure 1(c) shows the visualized flow pattern by a Schlieren method. The white and dark colored areas are the expansion and compression regions, respectively. The flow pattern by numerical analysis can express well the experimental one.

Figure 2 shows the pressure distribution P_s/P_0 on the side wall for the offset distance of $D/b = 3.0 - 7.0$. The pressure corresponding the vortex region is negative and it takes a maximum around the reattachment point, R.P (Fig. 1(a)). The position of the maximum pressure x/b moves to the downstream and the maximum pressure decreases as increasing the offset distance D/b. The numerical analysis can express well the experimental results.

Figure 3 shows the pressure fluctuation at $x/b = 16.4$ near the reattachment point, R.P. (Fig. 1(a)). The pressure fluctuates irregularly with the dominant frequencies of $f_d = 8.6$ and 19.0 kHz. This means that the reattached jet flows under the fluctuation with the same dominant frequencies.

Fig. 1: Supersonic under-expanded reattached jet ($P_0 = 0.4$ MPa, $D/b = 5.0$)

References

[1] Bourque, C. and Newman, B.G., Reattachment of a 2-D, incompressible jet to an adjacent flat plate, *Aeronautical Quarterly.*, 1960, **11**, 201-232.

Fundamental Study on Design Methodology of a Solar Car Considering Aerodynamic and Power Generation Performance

Arata Muto[1*], Ichiro Uto[2] , Kota Fukuda[3] , Kouhei Sagawa[4] and Hideki Kimura[4]

[1]*Course of Mechanical Engineering, Graduate School of Engineering, Tokai University*
[2]*Department of Human and Information Science, School of Information Science and Technology, Tokai University*
[3]*Department of Aeronautics and Astronautics, School of Engineering, Tokai University*
[4]*Department of Electrical and Electronic Engineering, School of Engineering, Tokai University*
4-1-1 Kitakaname, Hiratsuka, Kanagawa, 259-1292, Japan
* Corresponding Author: 0CEMM082@mail.u-tokai.ac.jp

Recently, various fuel efficiency standards for the automobiles have been disclosed in many countries in order to achieve net-zero carbon dioxide emissions and realize Carbon-Neutral, Carbon-Free Society. For these reasons, many electric vehicles have been developed and automobile manufacturers have tried to improve the fuel efficiency of automobiles. Bridgestone World Solar Challenge (BWSC) is one of international solar car challenges and a competition of technologies on eco-friendly car. The Tokai University Solar Car Team has participated in the BWSC in the past years. The distance of the BWSC is around 3,000 km and only energy obtained from sunlight can be used.

For the development of solar cars, the power consumption should be reduced since the solar power density is very low. Furthermore, the balance between power generation and aerodynamic performance is crucial for the design of the solar car. Therefore, in this study, a design methodology was proposed and applied to a solar car, called 2019 Tokai Challenger which Tokai University Solar Car Team developed for the BWSC 2019. In the methodology, both aerodynamic performance and power generation performance are considered by combining the flow simulation and a power generation simulation. By using the proposed methodology, total performance can be evaluated. Fig.1 shows the solar car, 2019 Tokai Challenger. The length is 5.0 m, the width is 1.2 m, and the height is 1.0 m. The cruising speed at the challenge was about 90 km/h.

Fig.1 2019 Tokai Challenger

In the aerodynamic simulation, the RANS simulation was carried out. Various shapes were proposed based on the simulation results. For the proposed shapes, the power generation simulation was conducted based on the analyzed wind velocity distribution and PV cells temperature distribution. Fig.2 shows comparison results of canopy shapes. The canopy shape influences both the aerodynamic characteristics and solar generation power reduction by shadow on solar array Fig.3 shows temperature distribution

on the solar array surface. These effects can be predicted by the flow simulation.

The solar generated power of each cell has been evaluated by considering the global irradiation based on direct solar irradiation, diffused solar irradiation, and cell angle.

By combining these simulations, both aerodynamic performance and power generation performance can be examined. In the BWSC 2019, the Tokai University Solar Car Team finished the second place. In this study, the fundamental methodology was proposed and applied to the development of 2019 Tokai Challenger. The results showed that the methodology is effective to develop high performance solar cars.

At the conference, the detail results of flow simulation and power generation estimation will be presented, and the detail of proposed design methodology will be explained.
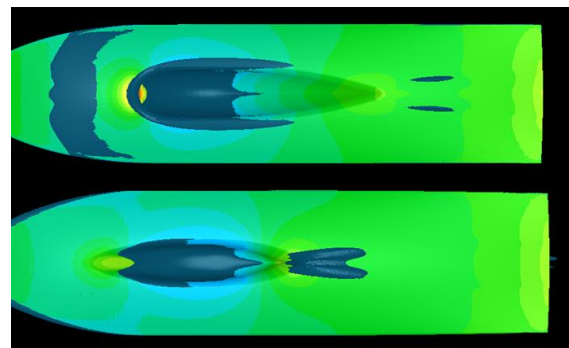
Fig.2 Surface pressure distribution and iso-surface of turbulent kinetic energy (Comparison of canopy shape)
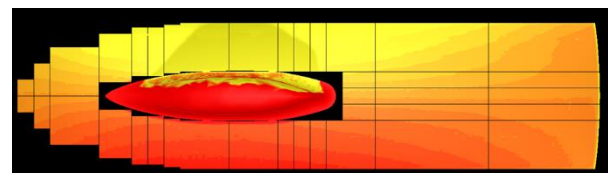
Fig.3 Temperature distribution at solar cell surface (Upper Surface)

Study on Drag Reduction of Superstructure of Ships and Improvement of Fuel Consumption

Kodai Fukushima[1], Kota Fukuda[2], Takao Kashiwagi[3], Takashi Danno[4], Koeki Onishi[5], and Koyu Kimura[6]

[1]Tokai University, 1cemm080@mail.u-tokai.ac.jp, Kanagawa, Japan
[2]Tokai University, fukuda@tokai-u.jp, Kanagawa, Japan
[3]Mitsui O.S.K.Lines, Ltd., takao.kashiwagi@molgroup.com, Tokyo, Japan
[4]Mitsui O.S.K.Lines, Ltd., takashi.danno@molgroup.com, Tokyo, Japan
[5]Mitsui O.S.K.Lines, Ltd., koeki.onishi@molgroup.com, Kanagawa, Japan
[6]Akishima Laboratories (MITSUI ZOSEN) Inc., kimurak@ak.mes.co.jp, Tokyo, Japan
* Corresponding Author: 1cemm080@mail.u-tokai.ac.jp

Large ships used in service for international freight are composed of a hull and a superstructure. The superstructure is a huge structure equipped with ship bridge, living environment of crew and so on. Consequently, a large aerodynamic drag force is generated by the superstructure. Various pioneering works on reduction of frictional drag of ships below the waterline have been carried out (for example, [1]). Bulbous bows have been used to reduce the interference of waves and drag force [2]. On the other hand, there are few studies on the reduction of aerodynamic drag force of superstructures.

For these reasons, in this study, some aerodynamic parts were proposed to reduce drag force of superstructure of ships based on our group's previous research [3]. The effects of aerodynamic parts were examined by wind tunnel test and numerical simulation. At first, the validation of the numerical simulation was carried out by comparing with the experimental data. Fig.1 shows the shape of the superstructure. Fig.2 shows the comparison results. The analyzed data is in good agreement with the wind tunnel data and the effect of aerodynamic parts are reasonably simulated. Furthermore, the detail effect of the aerodynamic parts and flow characteristics were investigated by numerical simulation. Fig.3 shows the simulation results in case of yaw angle = 0 [deg]. The results show that the wake and high turbulent energy region are reduced by installing the aerodynamic devices. More detail characteristics of vortical flow around the aerodynamic parts will be presented in the conference.

Furthermore, the fuel consumption in the actual sea route was evaluated by using the obtained data. The JPN-PG route was used as the target route. Fig.4 shows comparison between estimated braking horsepower (BHP) and the relative wind direction [deg]. In the case that the relative wind direction is from 0 [deg] to 90 [deg], the braking horsepower of Type A and B was decreased from the base model. By using the simulation results, the improvement of fuel consumption by the aerodynamic parts was examined. The detail results will be presented in the conference.
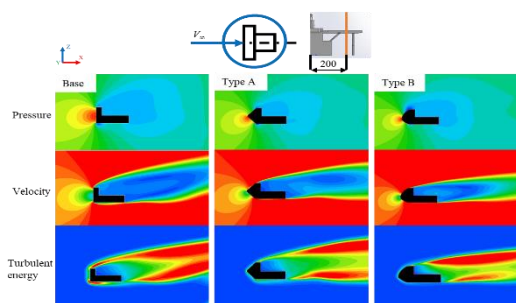
Fig.3 Flow patterns

(a): Full   (b): Ballast
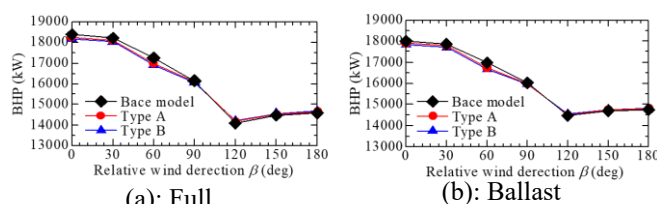
Fig.4 BHP value for each relative wind direction

References

[1] Koji Takahashi, Akira Kadokawa, and Yoshiaki Kodama, "Flow direction distribution of frictional resistance reduction by microbubbles", Proceedings of the Japan Shipbuilding Society, 1997 (in Japanese).

[2] Takeo Inui, Tetsuo Takahei, and Michio Kumano, "Tank Tests on the Effect of a Spherical Bow on Wave Formation", Proceedings of the Japan Shipbuilding Society, 1960 (in Japanese).

[3] Hiroki Yanagisawa, "Numerical Simulation on Resistance Reduction of Superstructure of Ship", Tokai university master's thesis, 2020 (in Japanese).

Fig.1 Shape of superstructure (Base model)

(a): Base model   (b): Type A   (c): Type B

Fig.2 Cf_x and Cf_y at each yaw angle (comparison between wind tunnel test and numerical simulation)

Keynote Lecture

Frank Holzäpfel
Senior Scientist (Dr.-Ing. habil.)
Institute of Atmospheric Physics
German Aerospace Center, Germany

Dr.-Ing. habil. Frank Holzäpfel graduated as a mechanical engineer from the University of Karlsruhe (TH) in 1990. He then specialized in measurement and modelling of turbulent swirling flows at the Engler Bunte Division of Combustion Technology in Karlsruhe, where he obtained his Dr.-Ing. in 1996. In 1997 he became a Research Scientist at the Institute of Atmospheric Physics, DLR (German Aerospace Center) in Oberpfaffenhofen, where he concentrates on wake vortex research, including large eddy simulation, real-time wake vortex model development, field experiments, wake vortex advisory systems, risk analysis, and wake vortex decay enhancement. In 2005 he obtained his Habilitation in Fluid Dynamics at the Faculty of Mechanical Engineering of the Technical University Munich where he was an associate lecturer from 2007 to 2009. In 2014 he was awarded the title Senior Scientist.

Lecture title:
Mitigating Aircraft Wake Vortex Risks During Final Approach via Plate Lines
by Frank Holzäpfel, Anton Stephan, Grigory Rotshteyn, Dennis Vechtel

Mitigating Aircraft Wake Vortex Risks During Final Approach via Plate Lines

Frank Holzäpfel[1*], Anton Stephan[1], Grigory Rotshteyn[1], Dennis Vechtel[2]

[1]*Deutsches Zentrum für Luft- und Raumfahrt, Institut für Physik der Atmosphäre, 82234 Oberpfaffenhofen, Germany*
[2]*Deutsches Zentrum für Luft- und Raumfahrt, Institut für Flugsystemtechnik, 38108 Braunschweig, Germany*
* *Corresponding Author:* frank.holzaepfel@dlr.de

As an unavoidable consequence of lift, every flying vehicle generates counter-rotating regions of turbulence known as wake vortices (see Fig. 1). These long-lived trailing vortices constitute a potential threat to following air traffic. Aircraft must therefore keep to a predetermined minimum separation distance. These aircraft separations limit the capacity of congested airports in a basically rapidly growing aeronautical environment. Decades of research on effective aircraft modifications aiming at the alleviation of the wake vortex hazard did not lead to operational use until today.

Fig. 1: Numerical simulation of wake vortex evolution generated by landing A340 aircraft with plate line.

The highest risk to encounter wake vortices prevails in ground proximity, where the vortices cannot descend below the glide path but tend to rebound due to the interaction with the ground surface. Weak crosswinds may compensate the self-induced lateral propagation of the upwind vortex, such that it may hover over the runway directly in the flight path of the following aircraft. That's why aircraft experience wake vortex encounters time after time, even under adherence to separation standards.

So-called plate lines mitigate the risk of wake vortex encounters during final approach and may help to enhance runway capacity. One plate line consists of several upright plates that are installed underneath the approach glide path at the ends of runways (Figs. 1 and 3). Plate lines are passive, cost-effective, robust and safe.

Since the first idea developed in the year 2008, the functionality of the patented plate lines was first demonstrated in towing tank experiments [1]. Next, using high-performance numerical simulations, the underlying physical mechanism was analyzed in detail, the size of the plate lines was optimized, and the influence of wind was investigated [1]. Flight tests with the DLR research aircraft HALO (Gulfstream G550) at the special airport Oberpfaffenhofen showed that the lifetime of the longest-lived vortices can be reduced by about 30%.

When a vortex gets close to the plates, strong Ω-shaped secondary vortices (SV) are induced at the plate's surface that actively approach the wake vortices (WV) by self-induced motion, (see Fig. 2, left). Then the secondary vortices are wrapped around the wake vortices by the primary wake vortex flow (Fig. 2, center). Finally, the secondary vortices propagate along either side of the wake vortices again driven by self-induced motion and accelerate their decay (Fig. 2, right). In Fig. 2 curved arrows denote the rotational direction of the vortices while straight arrows denote their self-induced directions of propagation.
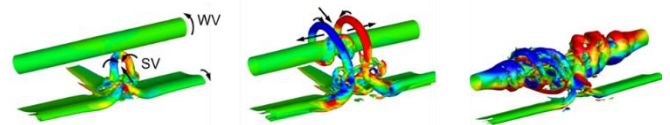
Fig. 2: Ω-shaped secondary vortex (SV) approaches wake vortex (WV) and wraps around it leading to premature wake vortex decay [1].

In the year 2019, the effectivity of the plate lines was demonstrated in a large-scale measurement campaign at Vienna International Airport [2]. Two temporary plate lines were installed underneath the glide path to runway 16. During a six-month period, wake vortex decay was measured for 9473 landings using lidar. It was found that plate lines reduce the lifetime of the most safety-relevant wake vortices by 22% for Medium category aircraft and by up to 37% for Heavy category aircraft. Depending on the aircraft pairing, plate lines allow for a potential separation reduction of 12% to 20% compared to the RECAT-EU separation scheme.

Fig. 3: Overflight of A380 of one of the experimental plate lines installed at runway 16 of Airport Vienna.

References

[1] Stephan, A. et al. (2014). Enhancement of aircraft wake vortex decay in ground proximity, CEAS Aeronautical Journal, 5, 109-125, http://dx.doi.org/10.1007/s13272-013-0094-8.

[2] Holzäpfel, F. et al. (2021). Mitigating Wake Turbulence Risk During Final Approach via Plate Lines, AIAA Journal, accepted, https://doi.org/10.2514/1.J060025.

Comparison of Synthetic Inflow Generation Methods for Atmospheric Boundary Layer Flows

Henry Plischka[1*], Johann Turnow[1], Nikolai Kornev[1]

[1]University of Rostock, Albert-Einstein-Str. 2,
18059 Rostock, Germany
* Corresponding Author: henry.plischka@uni-rostock.de

Large-eddy simulation (LES) has become a very prominent numerical tool for studying transport processes in the atmospheric boundary layer during the last 50 years [Stoll 2020]. More recently, due to increasing computational resources, also the urban boundary layer including dispersion processes is investigated with LES in academic researches. In non academic applications, on the other hand, such as the security analysis of gas propagation due to hazardous incidents, more simple models are commonly used. Primary due to the high computational costs LES is rarely used in industrial applications, although the prediction accuracy of the complex transport mechanism in densely build-up environments can verifiably be increased (e.g. [2]). One obvious instrument to reduce the calculation time and make LES for hazardous gas propagation more attractive is the use of synthetic inflow boundary conditions.

In this study a comprehensive analysis of several turbulent inflow conditions for the simulation of atmospheric boundary layer flows in rough environment is presented. Besides cyclic boundary conditions with a rough wall function at the ground, five synthetic turbulence generators (TG) of varying complexity, here referred to as TG1 [3], TG2 [4], TG3 [5], TG4 [6] and TG5, a simple random velocity field generator, are analyzed. The dependency to the required input Reynolds stresses, obtained either from previous LES or RANS simulations, are compared. Vertical profiles of the velocity and the normal stresses for two roughness lengths (z_0=0.06 m and z_0=0.29 m) as well as their alteration in stream-wise direction are compared with measurement data from the open-return boundary layer wind tunnel facility of the Meteorological Institute of the University of Hamburg. The vertical momentum flux, the integral length scales and the energy spectra are discussed as well.

Major differences can be observed between the results of the used turbulence generators. The inflow length, where the velocity profile alters from the input logarithmic profile to a stable state, as well as the final velocity profile in the near ground region strongly depend on the synthetic inflow method. It can be seen, that in case of higher roughness the final velocity profile is obtained faster for all methods. The prediction accuracy of the final profile of the particular method, however, depends unequally on the roughness length. The synthetic turbulence also shows strong disparities between the methods, where the best comparison with cyclic boundary conditions are obtained with TG1 and TG2.

The results show, that particular synthetic inflow methods with reasonable short inflow lengths can generate velocity and turbulence profiles which are in good comparison with experimental data.
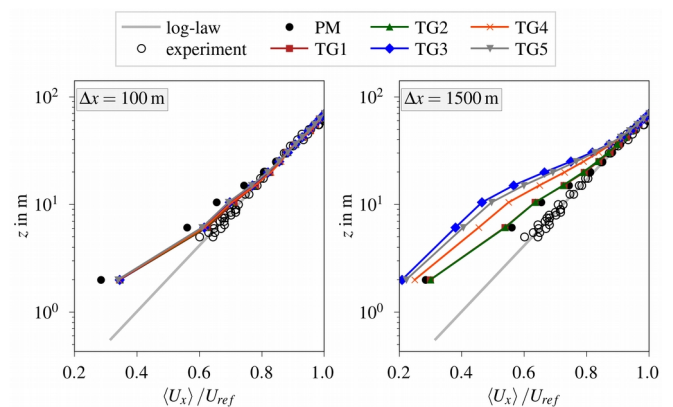
Fig. 1: Velocity profiles of five synthetic inflow generation techniques for z_0=0,06 m with a distance of 100 m (left) and 1500 m (right) downstream the inlet.

References

[1] Stoll R, et al. "Large-eddy simulation of the atmospheric boundary layer". Boundary-Layer Meteorology 177.2 (2020): 541-581.

[2] Tominaga, Y and Stathopoulos T. "CFD modeling of pollution dispersion in building array: evaluation of turbulent scalar flux modeling in RANS model using LES results". Journal of Wind Engineering and Industrial Aerodynamics 104 (2012): 484-491.

[3] Kröger H and Kornev N. "Generation of divergence free synthetic inflow turbulence with arbitrary anisotropy". Computers & Fluids 165 (2018): 78-88.

[4] Klein M, Sadiki A and Janicka J. "A digital filter based generation of inflow data for spatially developing direct numerical or large eddy simulations". Journal of computational Physics 186.2 (2003): 652-665.

[5] Xie, Z-T and Castro I P. "Efficient generation of inflow conditions for large eddy simulation of street-scale flows". Flow, turbulence and combustion 81.3 (2008): 449-470.

[6] Jarrin N et al. "A synthetic-eddy-method for generating inflow conditions for large-eddy simulations". International Journal of Heat and Fluid Flow 27.4 (2006): 585-593.

Identification and Analysis of vortical structures over an airliner's wing-fuselage junction

Stylianos Adamidis[1, 2], Nicholas C. Markatos[1, *]

[1]*National Technical University of Athens, Athens, Greece*
[2]*Hellenic Air Force, Athens, Greece*
* Corresponding Author: n.markatos@ntua.gr

Turbulence and flow disturbances occurring at the wing-fuselage junction of aircraft cause a drop in its aerodynamic performance and an increase in the aircraft's drag force. The main objective of this work is to study the junction flow's characteristics and the vortices, which dominate such flows. The flow condition corresponds to 5 degrees angle of attack with freestream Mach number of 0.189 and a Reynolds number based on the root chord of 2.43 million. The study is carried out using LES computational modeling and various sub-grid models. Specifically, this research study proposes a new junction flow parameter employed, in combination with the existing ones, in order aircraft designers to be able to assess more efficiently the horseshoe vortex behavior on the junction designs; and it is focused on the junction flow's and its vortices' characteristics, under the prism of vortices' structure formation and the flow patterns.

It is a fact that the majority of the junction flow studies focus on the horseshoe vortex considering it as the dominant vortex structures and many modern studies investigate the corner separation formation. The current study verifies the former vortices domination on these flows, but it also gives a more extended view, showing that all the vortex structures interact among themselves and form the junction flow regime.

Vortex Dynamics Effects on the Development of a Confined Wake and a Channel Flow in a Rectangular Duct Under Identical Inlet Flow Conditions

Ioannis Kalogirou*

Laboratory of Heating-Cooling & Refrigeration Dept of Mechanical Engineering Univ. of Peloponnese, Patras, Greece
* Corresponding Author: kalogirou@uop.gr

A circular cylinder turbulent wake developing in a confined flow environment, corresponding to a blockage ratio of 14%, has been studied experimentally in a wind tunnel comprising a parallel section followed by a constant area distorting duct. Near field measurements indicate that the confined wake exhibits to a certain extent similarity to the unbounded case with some differences, the most important being the modification of the Kármán Street topology. Further downstream, the confined wake velocity distributions demonstrate resemblance to channel flow behavior. Comparison of bounded wake and channel flow measurements, (taken in the absence of the cylinder), both obtained in the same apparatus under identical inlet flow conditions, has been also carried out. This procedure serves to elucidate the influence of near field formation dynamics on the far field structure with and without the presence of a bluff-body.

Wake measurements covered the Reynolds number range, (based on the cylinder diameter d), of $1.9 \times 10^3 \leq Re_d \leq 1.5 \times 10^4$. Some additional measurements were taken in the absence of the cylinder, (channel flow), at $Re_h = 15630$, h=21 mm being the channel half height. Here three-dimensional quantitative wake and channel flow data for $Re_d = 4300$ and $Re_h = 15630$ respectively, both obtained with the same free-stream centreline velocity $U_r = 11.25$ ms^{-1}, are presented. Additionally, qualitative results (flow visualisation) for the confined wake at $Re_d = 760$ are presented.

Fig. 1: Visualization of the near vortex street in the region $x_1/d = 0$-26.

A general view of the near wake region is shown in Fig. 1. A characteristic of the confined wake is the observed transposition of vortices. An upward movement of counterclockwise vortices with positive circulation to the upper midplane of the flow occurs. Simultaneously, countermotion of eddies with negative vorticity across the symmetry axis towards the lower half of the street takes place.

The vortex street reversal described above controls the evolution of the confined wake flow. The obtained near field mean profiles, shown in Fig. 2, exhibit "velocity deficit" distributions do not persist indefinitely. For $x_1/d > 60$ the mean velocity distributions differ markedly from those attained in the near wake region. Figure 3 compares a distant confined wake mean velocity profile with a corresponding channel flow one, under identical inlet flow conditions. Figure 4 shows autocorrelation functions for bounded wake and

channel flow as well. The changes observed in the two latter figures are attributed to basic differences in the vortex dynamics prevailing in the respective flow cases.
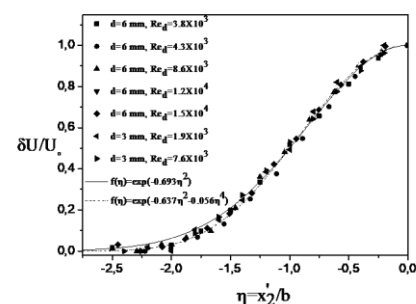
Fig. 2: Near wake similarity.
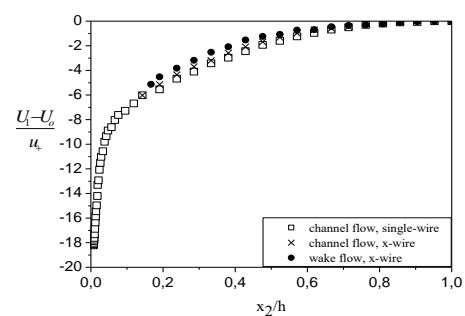
Fig. 3: Mean streamwise velocity distributions for confined wake and channel flow close to the end of the parallel section, ($x_1/d = 119.3$), in channel coordinates.
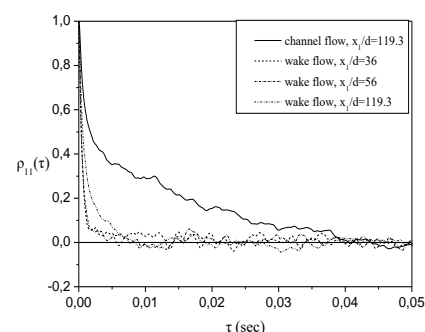
Fig. 4: Off-axis, ($x_2/h = 0.71$), autocorrelation functions of the streamwise velocity fluctuations for confined wake and channel flow along the parallel section.

References

[1] Taniguchi, S. and Miyakoshi, K. Fluctuating fluid forces acting on a circular cylinder and interference with a plane wall. Experiments in Fluids, 1990, 9:197-204.

The Numerical Simulation of the Vortex Shedding Flow from Two Circular Cylinders of the Parallel Arrangement in the Lock-in State in the Different Mode

Yoshifumi Yokoi[1*]

[1]*National Defense Academy of Japan,1-10-20 Hashirimizu, Yokosuka, Japan*
* Corresponding Author: yokoi@nda.ac.jp

This study carries out the numerical simulation of the interference vortex flow when varying the interval of two circular cylinders in a natural lock-in state (Karman vortex shedding) and two kinds artificial lock-in state (an alternate vortex shedding and simultaneous vortex shedding) using a vortex method. The purpose of this research is to investigate the mutual interference flow characteristic from the circular cylinder in mutually different lock-in mode. It is the enjoyment of this study to investigate how the artificial lock-in state influences the natural lock-in state (Karman's vortex discharge). It is very interesting to know how the vortex flow in which it interfered will change. The research was carried out by numerical simulation by use of vortex method.

The numerical experiment apparatus was consisted of simulation software and a notebook type computer as calculation hardware which are on the market. The software used vortex method which is based on the Lagrangian analysis. The vortex method is a direct viscid-inviscid interaction scheme, and the emanation of velocity shear layers due to boundary layer separation is represented by introduction of discrete vortices with viscous core step by step. In the present study, the calculations were performed at the two-dimensional flow field for incompressible and viscous flow. Two circular cylinders have been arranged right-angled to a flow. Here, the circular cylinder located in left-hand side toward the flow was called the 1st cylinder, and the circular cylinder located in right-hand side toward the flow was called the 2nd cylinder. The cylinder diameter d and the main flow velocity U were determined as 16 mm and 0.04 m/s so that it could compare with the previous experimental result [1]. Here, the diameter of two circular cylinders is the same. Since water is assumed as for test fluid, Reynolds number Re becomes 500. The configuration of circular cylinder was represented 40 vortex panels using a boundary element method. Every calculation continued to until non-dimensional time $T = 200$.

The main parameters of numerical experiment were the existence of oscillation, the oscillation frequency ratio f/f_K, the oscillation amplitude ratio $2a/d$ and the distance ratio L/d. Existence of the oscillation is 2 kinds and they are in the states of cylinder stationary and cylinder oscillation. The oscillating frequency ratio f/f_K is 2 kinds and they are in two typical lock-in states of the single oscillating circular cylinder obtained from the previous experimental result. As for the oscillating frequency ratio, $f/f_K = 1.4$ and $f/f_K = 2.4$ were used. Here the natural Karman vortex shedding frequency was $f_K = 0.6489$ Hz. The oscillation amplitude ratio $2a/d$ is 2 kinds, and they are 0.25 and 0.50, respectively. The distance ratio L/d is 5 kinds and they are 1.5, 2.5, 5.5, 10.0 and 20.0.

In order to investigate the aspect of interference by the natural lock-in and two kinds of the artificial lock-in, it calculated by varying the distance ratio of parallel two circular cylinders. As an example, the aspects of the interference flow of the natural lock-in and the artificial lock-in in amplitude ratio $2a/d = 0.5$ are shown in Figs. 1 and 2, respectively. The distance ratio L/d is changed in those figures. If the distance ratio becomes small, the vortex shedding from two circular cylinders can be seen become a complicated flow by mutual interference. Although the vortex shedding in the artificial lock-in state of the alternate vortex shedding type is influenced by change of the distance ratio, even if, as for the vortex shedding in a simultaneous vortex shedding type lock-in state, the distance ratio changes, the vortex shedding is carried out simultaneously. If the interval of two circular cylinders is narrow, the vortex streets discharged from each circular cylinder will unite. It was found that the alternate vortex shedding type lock-in receives interference by cylinder arrangement. In the case of such a complex state, it became clear to completely differ from the result obtained when the aspect and fluid force of the flow are single.

(a)   (b)   (c)
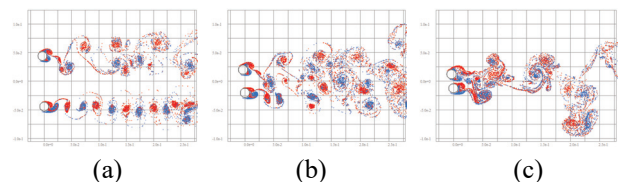
Fig. 1: Instantaneous flow feature in the case of 'Alternate lock-in vs. Natural lock-in' at the time T=200, (a) L/d=5.5, (b) L/d=2.5, (c) L/d=1.5

(a)   (b)   (c)
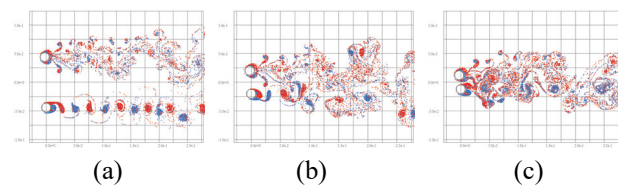
Fig. 2: Instantaneous flow feature in the case of 'Simultaneous lock-in vs. Natural lock-in' at the time T=200, (a) L/d=5.5, (b) L/d=2.5, (c) L/d=1.5

References

[1] Yokoi Y, Hirao K. Vortex Flow Around an In-Line Forced Oscillating Circular Cylinder. *Transactions of Japan Society of Mechanical Engineers* Series B, 2008, 74(746): 2099-2108.

Turbulent channel flow past a wall-mounted cuboid

Ariane N. R. Vieira[1*], Hendrik C. Kuhlmann[1], Johann Waringer[3], Carina Zittra[3], Jan Martini[3], Simon Vitecek[4], Stephan Handschuh[5]

[1]*Institute of Fluid Mechanics and Heat Transfer, TU Wien, Tower BA/E322, Getreidemarkt 9, A-1060 Vienna, Austria*
[2]*Department of Functional and Evolutionary Ecology, Division Limnology, University of Vienna, Althanstrasse 14, A-1090 Vienna, Austria*
[3]*WasserCluster Lunz, Dr. Carl Kupelwieser Promenade 5, A-3293 Lunz am See, Austria*
[4]*VetCore Facility for Research, Imaging Unit, University of Veterinary Medicine, Veterinärplatz 1, A-1210 Vienna, Austria*
[*]*Corresponding Author: ariane.vieira@tuwien.ac.at*

We investigate the incompressible turbulent flow past a wall-mounted square cuboid placed in a channel. Large Eddy Simulation (LES) is used in combination with the divergence-free synthetic eddy method (DFSEM) [1] to generate the turbulent inflow conditions. The geometry of the computational domain is shown in Fig. 1. To close the problem, we impose convective boundary conditions at the outlet, periodic boundary conditions in span direction, and no-slip conditions at the top wall, bottom wall, and all faces of the cuboid.
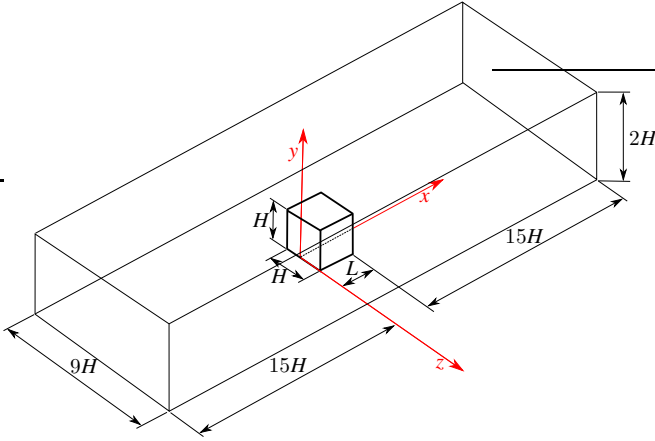
Fig. 1: Sketch of the geometry of the computational domain and coordinate system.

We validate the procedure by comparing with experimental data for a wall-mounted cube ($L = H$) and bulk Reynolds number $\mathrm{Re}_H = HU_b/\nu = 4 \times 10^4$ [2] (U_b: bulk velocity). Simulations are performed for bulk Reynolds number $\mathrm{Re}_H = 2 \times 10^4$, and for different length-to-height aspect ratios Γ of the cuboid in the range $0.25 \leq \Gamma \leq 6$. We compute the mean flow structures and the different separated regions.

A horseshoe vortex is formed in front and aside of the cuboid, as seen in Fig. 2. For $0.25 \leq \Gamma < 1.5$, its vorticity feeds, along with the shear layer from the top, the arch vortex in the wake. For $\Gamma > 1.5$, we observe a reattachment point on the sides of the cuboid and an alteration of some topological points: the two hyperbolic points, one beneath the cuboid and one in the wake, present when $\Gamma < 1.5$, merge into one. In addition, the separation point on the rear wall of the cuboid moves to the sidewall of the cuboid. Those alterations modify the footprint of the arch vortex from an almost circular shape to one elongated in the streamwise direction.

For small Γ the streamwise length of the mean wake recirculation bubble L_w decreases with Γ, reaching a minimum at $\Gamma \approx 2$. The length of the sidewall separation bubble L_s exhibits the opposite trend and reaches a maximum at $\Gamma \approx 2$. For $\Gamma \gtrsim 2$ the vortices shed from the sidewalls cause an increase of L_w, while L_s saturates. An increase of the channel height

from $2H$ to $4H$ reduces the size of the recirculation region at the top of the cuboid (not shown). Other than that, the flow structures remain almost the same.

(a) $\Gamma = 1.00$
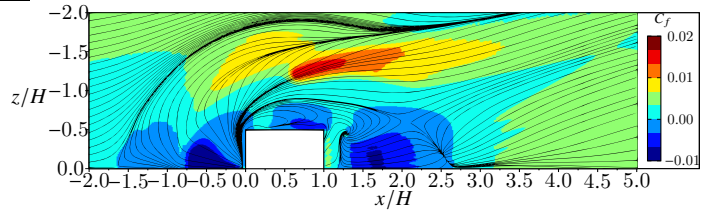
(b) $\Gamma = 1.25$
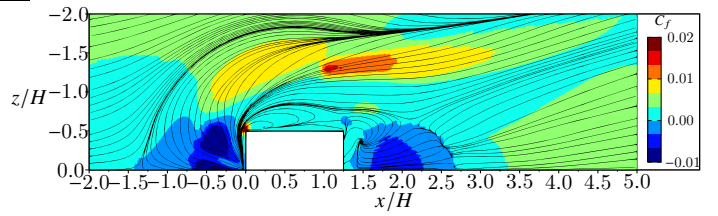
(c) $\Gamma = 2.00$
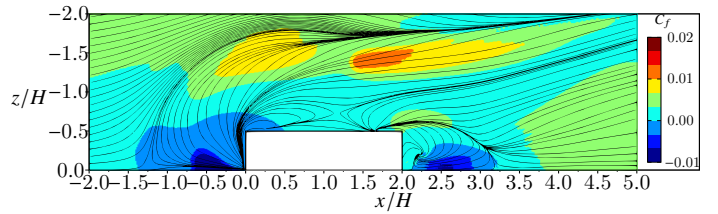
(d) $\Gamma = 3.00$
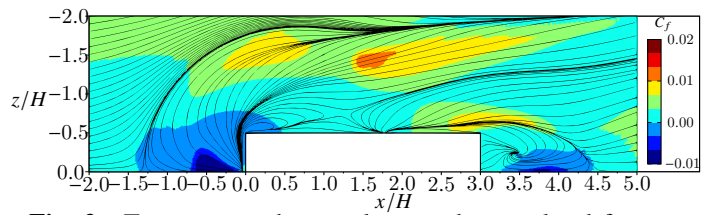
Fig. 2: Time-averaged streamlines and normalised friction coefficient (color) in the plane $y/H = 0.003$ from the bottom for different aspect ratios Γ.

Summarising, the dependence of the characteristic mean flow structures on the aspect ratio Γ of the cuboid have been established. The most sensitive vortical structure is the main recirculation bubble in the wake of the cuboid.

References

[1] Poletto R, Revell A, Craft T, A new divergence free synthetic eddy method for LES inflow boundary conditions, Flow Turbul. Combust. **91** (2013) 519-539.

[2] Martinuzzi R, Tropea C, The flow around surface-mounted, prismatic obstacles placed in a fully developed channel flow (Data Bank Contribution), J. Fluids Eng. **115** (1993) 85-92.

Numerical Investigation of a Backward Facing Step Flow Controlled by a Synthetic Jet

Dionysia Voultsou[1], Alexandros Romeos[2,1*], Alexandros Kalarakis[1], Athanasios Giannadakis[2,1]

[1]*Mechanical Engineering Dept., University of the Peloponnese, Patra, Greece*
[2]*Mechanical Engineering & Aeronautics Dept., University of Patras, Patra, Greece*
* Corresponding Author: *romaios@upatras.gr*

In the present work, the flow over a backward-facing step with the presence of a synthetic jet is studied using a 2D CFD model. The geometry under investigation can be found in numerous engineering applications in aeronautics and industry such as heat exchangers, nuclear reactors, diffusers, air conditioning systems. This study focus on recirculating flows detaching and reattaching to the main flow. Knowledge of the conditions under which these phenomena are observed helps in the development of flow control technologies and thus minimize flow disturbance, and kinetic energy losses.

Separation of the flow over the Backward Facing Step is created by a 2-D channel configuration (Fig. 1), resulting in the creation of evolving recirculation zones that reattach to the main flow. An active synthetic jet is situated, after the back face of step to control the evolution of the recirculation zones.
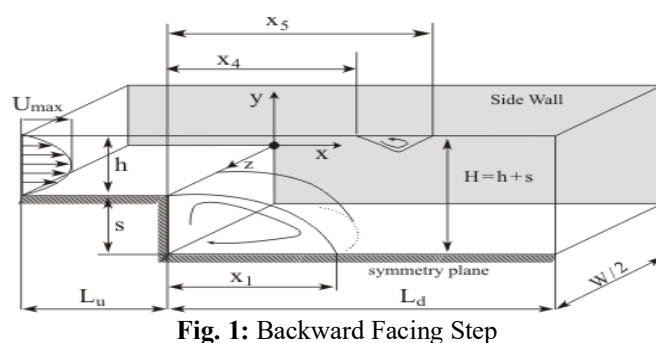
Fig. 1: Backward Facing Step

The operation of the synthetic jet is based on the periodic alternation between the suction and injection phases so that the mass supply to the main flow balance remains zero per period The motion of jet flow is caused by a diaphragm that moves periodically inside a cavity (Fig. 2).
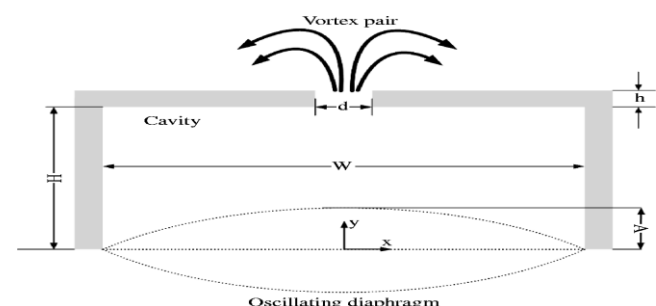
Fig. 2: Synthetic jet

Simulation the flow field, is realized via a K-ω SST turbulence model implemented on a tetrahedral structured mesh. The operating frequency of the synthetic jet is 90 Hz with a Strouhal number, $St = 0.03$. Typical images of synthetic jet flow evolution are presented in figure 3.
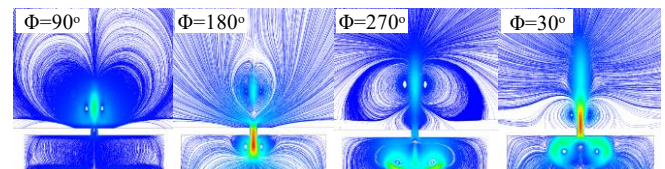
Fig. 3: Typical synthetic jet flow evolution at different pulse phases

At first, the numerical simulation study, is performed without the presence of the synthetic jet for several Reynolds number (Re=350-10000). Then, the influence of the synthetic jet on flow control is investigated. Characteristic velocity contours for the case of U=1 m/s bulk inlet velocity and Re=10000 are presented in figure 4.
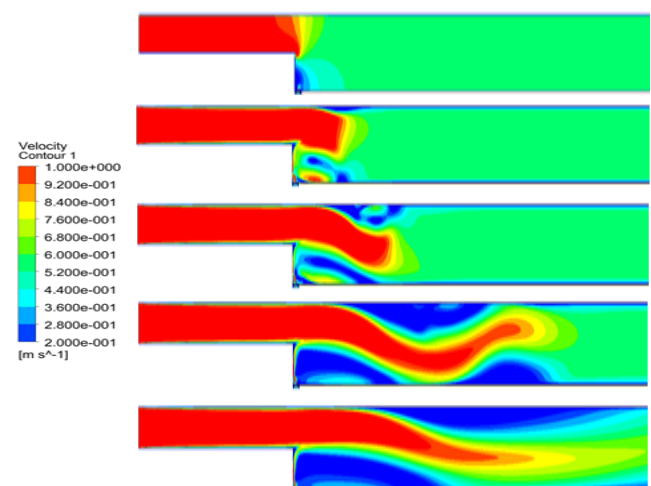
Fig. 4: Mainstream mean velocity contours at different time steps (t=0.01, 0.5, 1, 2, 4 sec)

References

[1] Strzelczyk P., Gil P., Properties of velocity in the vicinity of synthetic jet generator, Journal of Physics, 2016, (760).

[2] Li Z., Zhang D., Liu Y., Wu C., Gao N., Effect of periodic perturbations on the turbulence statistics in a backward-facing step flow, Physics of fluids, 2020, 32(7).

[3] Biwas G., Breuer M., Durst F., Backward-Facing Step Flows for Various Expansion Ratios at Low and Moderate Reynolds Numbers, J. Fluids Eng., 2004 (126(3).

An experimental study on the wake of a sphere having a uniaxial through-hole

Hayato Kato[1*], Kotaro Takamure[2],Tomomi Uchiyama[2]

[1]*Graduate School of Informatics, Nagoya University, Nagoya, Japan*
2Institute of Materials and Systems for Sustainability, Nagoya University, Nagoya, Japan
* Corresponding Author: kato.hayato@a.mbox.nagoya-u.ac.jp

We refer flows arise from bodies moving in stationary fluids or them placed in uniform flow to wake. Flows involving wake are frequently observed in our life exposed to various fluid environments and have big effects on circumstances surrounding us. So, it is very important to understand these characteristics. Many experiments about wake of a sphere [1] or a circular cylinder [2-3] were carried out so far. Effects of a bluff body shape on the wake were investigated. Igarashi [2-3] placed a circular cylinder having a slit within a uniform flow to investigate the effect of the slit angle on the wake of the circular cylinder. When the slit was parallel to the streamwise direction, the slit angle β equals to 0°. For $0° \leqq \beta \leqq 40°$, the self-injection jet from the slit into the wake was observed, and the resulting vortex formation region move downstream. For, $60° \leqq \beta \leqq 90°$, the boundary layer suction was observed periodically with the period of the vortex shedding. These results indicate the possibility to control the wake by modifying the body shape

This study placed a sphere having a through-hole within a uniform flow and explored the effects of the angle between the through-hole and the uniform flow direction on the wake of the sphere.

Fig.1 (a) shows an overview of the experimental setup. This experiment was performed using a wind tunnel. The dimension is 500 mm × 180 mm × 180 mm. A sphere was placed 125 mm away from the exit of the wind tunnel. The coordinate origin was the center of a sphere. X, Y, and Z represent the streamwise, spanwise, and vertical directions, respectively. Fig.1 (b) shows the definition of the angle of through-hole and the dimensions of the sphere. The sphere diameter d was 25.4 mm, and the through-hole diameter was 6mm. The angle α was 0° when the through-hole was set to be along the X axis. The flow velocity in the wake of the sphere was measured by a hot-wire anemometer (KANOMAX 7000ser.). In this experiment, a uniform flow velocity U_0 was 7 m/s and the Reynolds number based on d and U_0 was almost 12,000.

Fig.2 shows the spanwise distributions of the streamwise mean velocity normalized by d at $X/d = 1$. When $\alpha = 0°$, a jet from the through-hole was observed, and accordingly the velocity defect was the smallest. When $\alpha = 45°$, the velocity distribution was left-right asymmetry and the velocity defect was smaller locally near the edge of the through-hole. When $\alpha = 90°$, the velocity distribution was similar to that of a sphere without a through-hole, but the velocity defect was smaller. As stated above, the effect of a through-hole on the wake changes as a function of α.
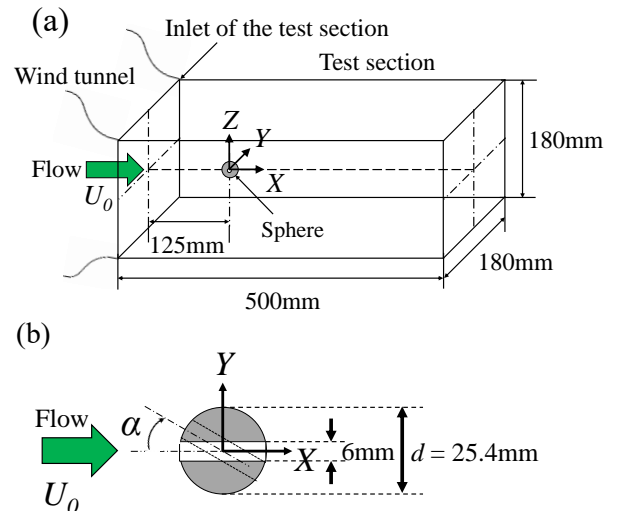
Fig.1: Schematic of the test section. (a) Overview of the experimental setup, (b) details of angle and dimension s of sphere and through-hole
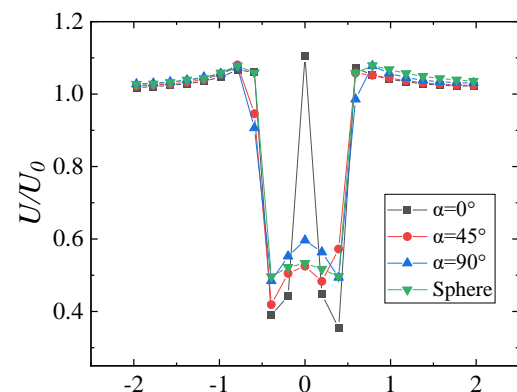
Fig.2: Spanwise distributions of streamwise mean velocity at $X/d = 1$

References
[1] E. Achenbach, "Vortex shedding from spheres." J. Fluid Mech., vol.62 (2), pp209–221(1974).
[2] T. Igarashi, "Flow Characteristics around a Circular Cylinder with a slit (1st Report, Flow Control and Flow Patterns) ,"Bulletin of the JSME, vol.21, No.154, pp154-16 (1978).
[3] T. Igarashi, "Flow Characteristics around a Circular Cylinder with a slit (2nd Report, effect of Boundary Layer Suction)," Bulletin of the JSME, vol.25, No.207, pp207-8 (1978).

Vortical systems, generated by Darrieus and Savonius Rotors

Dmytro Redchyts[1], Svitlana Moiseienko[2], Yevhenii Shkvar[3*], Shiju E[3]

[1]*Institute of Transport Systems and Technologies of the NASU, Pysarzhevskoho str., 5, Dnipro, Ukraine*
[2]*Kherson National Technical University, Beryslavske highway, 24, Kherson, Ukraine*
[3]*College of Engineering, Zhejiang Normal University, 688 Yingbin Road, Jinhua, China*
* Corresponding author: redchits_da@ua.fm

Aerodynamics plays the basic role in the operation of wind turbine. Final efficiency of wind turbine depends on optimization of a rotor form, aerodynamic qualities of rotating surfaces of the wind turbine itself. The simplicity and reliability of the vertical-axis wind turbines (VAWT), the ability to work under of conditions of moderate wind allows them to be installed in hard-to-reach areas of significant social importance.

It is well known that Darrieus rotors have superior power factors, which are still inferior to horizontal-axis wind turbines in terms of aerodynamic efficiency. Insufficient level of understanding of the aerodynamic processes of the VAWT plays a major role in such state of affairs. Another reason is the outdated methodology for development of industrial samples of high-power wind turbines which are based on empirical assumptions on the flow pattern around the VAWT rotors and discards adequate calculations of the blade aerodynamics for the case of dynamic stall.

This research considers the orthogonal Darrieus and Savonius rotors. The typical blades are much longer than the chord that allows to neglect end effects on blades and to take advantage of a hypothesis about plane-parallel structure of flow. Thus, the problem supposes two-dimensional statement in a plane which is perpendicular to the axis of rotor rotation. Wind turbine aerodynamic processes are described by incompressible RANS equations closed by Spalart-Allmaras eddy viscosity turbulence model as quite simple, reliable and appropriate for a wide range of external flows.

Flow visualization was performed for two-blade Darrieus rotor on the basis of physical [1] and computational experiments (Fig. 1). For greater clarity, only the vortices of maximum intensity are left. At the beginning of a leeward side of a trajectory and before angular position of a rotor two hundred and forty degrees the flow around the blade has the attached character. Separated flow appears at mentioned rotor angle (240º). As well as in case of dynamic stall on the inner surface, vortexes separate from a leading edge of the blade and begin movement along a surface.

For the considered parameters, the flow picture is characterized by essential unsteady phenomena such as: dynamic stall, generation of complex system of vortexes, interaction of vortexes of different sizes, speeds and intensities with the rotor surface.

This study gives the results of three series of computational experiments on aerodynamic and power characteristics of two and three-bucket Savonius rotor.

The first set of computational experiments was conducted for steady Savonius rotor which was fixed at various angles of attack. For the majority of angular positions the two-bucket Savonius rotor time-averaged torque coefficients are positive, but for angles 55-80º they are negative. For three-bucket configurations torque coefficients are always positive.

The second set of computational experiments was conducted for fixed tip-speed-ratio of Savonius rotor (Fig. 2). The maximum value of the torque coefficient is 0.4 for two-bucket and it is 0.35 for three-bucket Savonius rotor. They correspond to the tip-speed-ratio of 0.4. The maximum value of power coefficient is 0.23 for two-bucket and 0.19 for three-bucket Savonius rotor.

The third set of computational experiments corresponds to the coupled problem solution including dynamics and aerodynamics of three-bucket Savonius rotor. Calculations were carried out in three stages. The purpose of the first stage was to determine a periodic flow with a structure similar to the Karman vortex street. At the second and third stages, the coupled equations describing Savonius rotor aerodynamics and rotation were solved. After unlocking the rotor begins to rotate under effect of incoming wind flow that intensifies the vortexes formation. The frequency of vortex detachment depends on incoming flow velocity, characteristic dimensions and rotor rotation speed. At the third stage the torque of load is applied to the Savonius rotor that results in stabilization of rotor angular speed and near to cyclic variations of drag force, lifts force and torque coefficients.
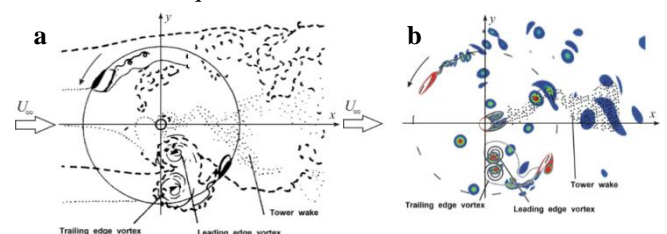
Fig. 1: Visualization of the flow field at operation of two-blades Darrieus rotor, based on physical [5] (a) and computational (b) experiments
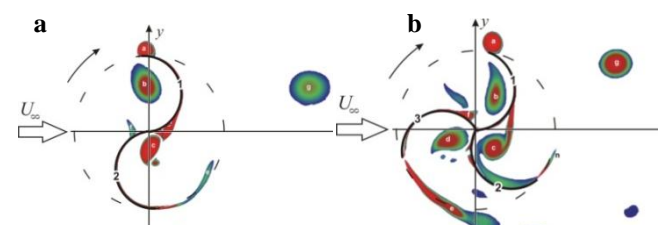
Fig. 2: Visualization of the flow field at operation of two-blades (a) and three-blades (a) Savonius rotor

References

[1] Brochier G., Fraunie P., et al. Water channel experiments of dynamic stall on Darrieus wind turbine blades [J]. Journal of Propulsion and Power, 1986, 5(2): 445-449.

The assessment of the impact of turbulence generated by wind turbines planned for construction in close proximity of high voltage power transmission lines on   the wind farm location problems

Waldemar Kamrat

Gdansk University of Technology, Faculty of Electrical and Control Engineering, Power Engineering Department, 11/12 Narutowicza Street, 80-233 Gdansk, Poland
* Corresponding Author: waldemar.kamrat@pg.edu.pl

The paper presents selected aspects of network construction related to the location of wind turbines due to their aerodynamic impact on power lines of high and highest voltage. Based on the source data concerning the aerodynamic impact of a wind farm consisting of eight turbines on a 400 kV transmission power line, an analysis of the possibility of wind farm locating in the immediate vicinity of the line was carried out.

One of the most important issues in the design/construction of wind farms is the rationalization of the typology of distribution of individual generating units due to the turbulence they generate [1]. There are many models (physical and mathematical methods) and the methods used to calculate the impact of turbulence on the efficiency of a wind farm. Their excellent characteristics are included in the work [2], where the currently used models and programs for numerical calculations are described. Reference [2] shows frequently used computational programs include: WAsP, WindPro, WindFarmer, WindFarm, WindSim, where respectively Jensen models [3] and the linearized CFD model are used, a module with WAsP; while the WindFarmer program uses the following models: Ainslie, RANS and CFD. On the other hand, the following models were used in the WindFarm software: Jensen, Ainslie and Larsen, and the models: Larsen [3],[4] and Ishikara [5] in the WindSim program, which give a relatively short computation time. Finite element methods are also used for modelling/calculating turbulence [6],[8],[9],[10].

These issues are the subject of this article, in which the author shows a case study set in a real decision-making situation. To illustrate the scope of research and analyzes - examples of illustrations of a turbulent vortex (see Fig. 1-2) are presented below, which were obtained for the object with the assumption that the wind blows from the left side to the right, the turbine stands on the X axis in position 0, and the 400 kV transmission power   line pole on the X axis at 250 meters (it is hardly visible because it is low compared to the turbine itself).

Fig. 2. Longitudinal section of a turbulent vortex [11]

References

[1] G. Crasto, *et al.*, *Wind turbines wake calculations. Comparins of actuator disc against analitycal models,* AWEA 2011. Wind Power Proceedings, Anaheim, California, 2011.

[2] A. Drozdowicz, *et al.*, *Badanie wpływu przeszkód na sprawność farm wiatrowych na modelach*, Poznan University of Technology Academic Journals - Electrical Engineering 2016 no. 87 (in Polish), Poznan Poland 2016.

[3] N. O. Jensen, *A note on wind generator interaction,* Technical Report Riso-M-2411, Roksikte, Denmark, November 1983.

[4] J. Choi, M. Shan, *Advancement of Jensen (Park) wake model*, Proceedings of the EWEA Annual Meeting, Vienna, 2013.

[5] T. Ishihara, A. Yamaguch, Y. Fujino, *Development of a new wake model based on a wind tunnel experiment*, Global Wind Power, 2004.

[6] S. Kleinstahl, J. Schwenk, *Effect of turbulence on high-voltage line*, ADC Report 2020-10, Rev.2.2. Feb.2020, Dynamik Consult, Neuhausen, Germany, 2020.

[7] C. Micaleff, *et al., The origins of wind turbine tip vortex,* Journal of Physics: Conference Series 555012074, 2014.

[8] K. Tesch, *Metody numeryczne. Podstawy modelowania turbulencji,* Zakład Mechaniki Płynów, Politechnika Gdanska (in Polish), Gdansk, Poland 2020.

[9] Source materials, Mashav Management Sp.z o.o. (in Polish -unpublished),Warsaw, Poland, 2020.

[10] W. Kamrat, *Own studies (2015-2020),* Katedra Elektroenergetyki (in Polish -unpublished). Politechnika Gdańska, Gdansk,   Poland 2020.

[11] W. Kamrat, *Selected problems of wind turbines location under wake conditions due to power transmission lines*, Elektroenergetyka, Vol. 1, No. 22, 2020.

Fig. 1. View of a turbulent whirl [11]

Vortical flows in the wake of bluff bodies and their role in flame anchoring.

Georgios Paterakis, Konstantinos Souflas, Evangelos Panagiotis Mitsopoulos, Eleni Manouskou, Panagiotis Koutmos

Laboratory of Applied Thermodynamics, Department of Mechanical Engineering and Aeronautics, University of Patras.
University of Patras, 26504, Patras Greece.
* Corresponding Author: epmitsopoulos@gmail.com

The time averaged and fluctuating flow field characteristics of vortical flows established downstream of a variety of axisymmetric baffles, have been investigated for a double-cavity fuel-air premixer/stabilizer arrangement, for isothermal and reacting conditions. The work aims to broaden knowledge regarding the impact of different bluff body shapes, leading and trailing edge contours, blockage ratios and incoming flow profiles, on the development of the downstream bluff body formed wake—vortex structures. Particle Image Velocimetry (PIV) measurements have been applied to obtain the mean and turbulent velocity fields throughout the afterbody near wake zone.
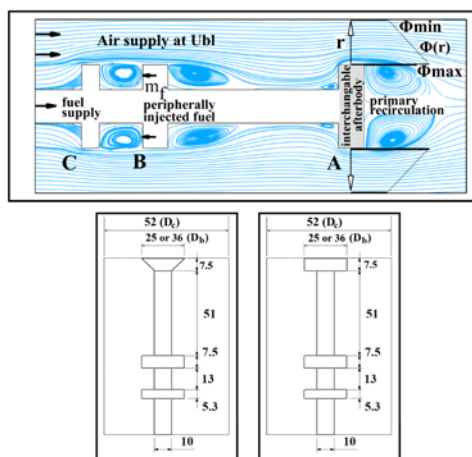
Fig. 1: Bluff body/burner configurations

The experimental facility is shown in Fig. 1 and has been described in detail in [1,2]. Three axisymmetric baffles (A, B, C) connected along their axis with a 10mm hollow tube comprise the premixer/burner arrangement. Two bluff body shapes and blockage ratios have been studied for both isothermal and reacting conditions. The stabilizing afterbody "A" is either a disk- (D) or cone- (C) shaped body, with a diameter of 25 or 36mm (D_b) and a rim thickness of 7.5mm, as shown in Fig. 1.

Measurements of the velocity fields have been conducted with a two-dimensional Particle Image Velocimetry configuration (2DPIV, LaVision® FlowMaster 2D) and described in detail in [3].

The results highlighted the importance of the velocity characteristics at the wake inlet zone as predisposed by the interaction of the trailing edge geometry with the upstream double cavity premixer, and the difference between geometric and aerodynamic bluffness for each bluff body.
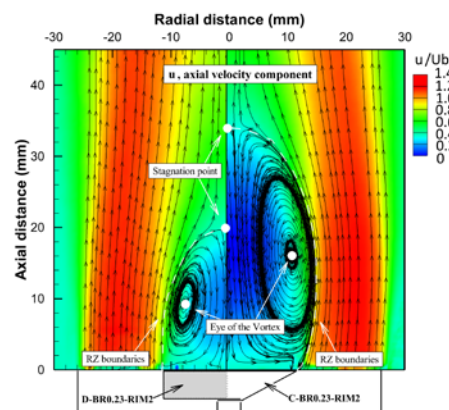
Fig. 2: Bluff body/burner configurations

Downstream of the cone shaped bluff bodies, larger recirculation zones have been encountered, For the same basic bluff body shapes, an increase in blockage ratio had a minor effect on the width of the RZ. Also, shifting from a cone to a disk shaped baffle, resulted in a reduction of the RZ length of about 29-35%. Finally, cone shaped bluff bodies produced, in general, total strain rate values of about 1.7 times greater that the disk shaped ones, for the same blockage ratios. The above information combined with the inlet fuel-air mixture topologies that emanate from the investigated premixer/burner set ups can provide important information on the interaction of fuel-air mixture disposition and the vortical flows established in the near wake zone. Such knowledge is crucial for the promotion of flame stabilization under operation with a variable range of fuel types.

References

[1] Karagiannaki C, Dogkas E, Paterakis G, Souflas K, Psarakis EZ, Vasiliou P, et al. A comparison of the characteristics of disk stabilized lean propane flames operated under premixed or stratified inlet mixture conditions. Exp Therm Fluid Sci 2014;59. doi:10.1016/j.expthermflusci.2014.04.002.

[2] Paterakis G, Politi E, Koutmos P. Experimental investigation of isothermal scalar mixing fields downstream of axisymmetric baffles under fully premixed or stratified inlet mixture conditions. Exp Therm Fluid Sci 2019;108:1–15. doi:10.1016/j.expthermflusci.2019.05.018.

[3] Banyon C, Rodriguez-Henriquez JJ, Paterakis G, Malliotakis Z, Souflas K, Keramiotis C, et al. A comparative study of the effect of varied reaction environments on a swirl stabilized flame geometry via optical measurements. Fuel 2018;216. doi:10.1016/j.fuel.2017.09.105.

ICVFM 2021

9th International Conference on Vortex Flow Mechanics

11-13 October 2021, Virtual Conference, University of Patras, Greece

Virtual Conference Guidelines

Guidelines to participate to the virtual conference

- The virtual conference will take place on the Zoom meeting platform.

- You will receive the meeting link via e-mail. No passcode is required to join the meeting.

- Clicking on the link you will be able to join the conference room through your internet browser. If you don't have Zoom Client installed, the browser page will also provide a download link for the software.

- We recommend you download and install the Zoom client software to use the full capabilities of the platform. Participants who are unable to install Zoom, can join the conference room using the Zoom web client on their desktop web browser. The Zoom web client offers limited functionality. The Join from your browser link will appear after the user clicks the link to join the meeting.

- Make sure that you join the conference room, with your name written with Latin characters. You may rename your ID right clicking on your thumbnail.

- Zoom meeting platform can be accessed on your personal computer, tablet or even smartphone. We suggest you log in through your personal computer for more easier handling of platform settings.

- The pre-recorded oral presentations of each paper will be played by the technical support team of the conference. No action of the speakers is required.

- Speakers/chairs should test their microphones, speakers, and cameras. They are recommended to enable their camera and microphone during the discussion of their presentation. For any technical issue the support team will help you to enable your microphone and camera. The use of earphones can eliminate external noise.

- During the discussion speakers are also recommended to have their presentation open on their personal computer. They may need to share their screen and navigate through their presentation to answer questions stated in the chat.

- Participants should disable their camera and microphone during the conference.

- Participants should use the chat to post their questions and comments. During the discussion, the chair of each session will pose the questions of the participants to the speakers.

- The conference link will be active each day, one hour before the start of the conference sessions. Participants may test their connectivity during these intervals.

Zoom Meetings platform functionality

Meeting room:

When you join the meeting room you can use the available menu options.

You can change your meeting view by clicking the view button on the top right side.
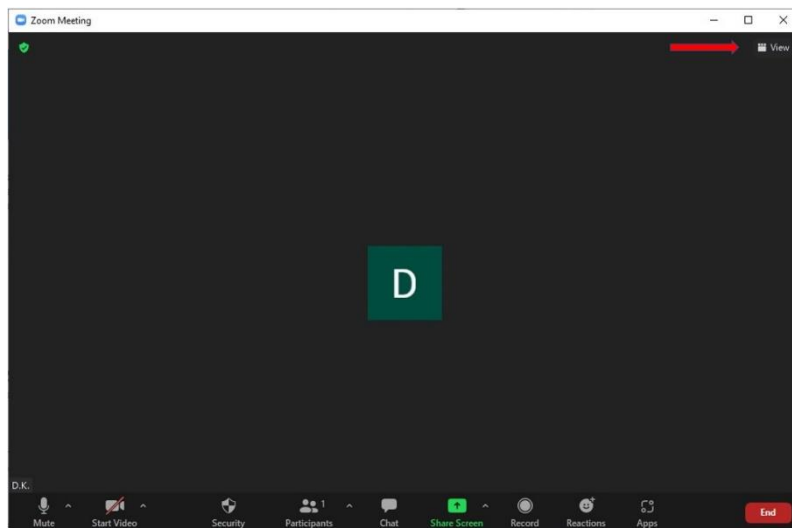
Camera and Video Settings:

Speakers/chairs can enable their camera during their presentation by clicking the Start Video button on the left bottom side of the platform.
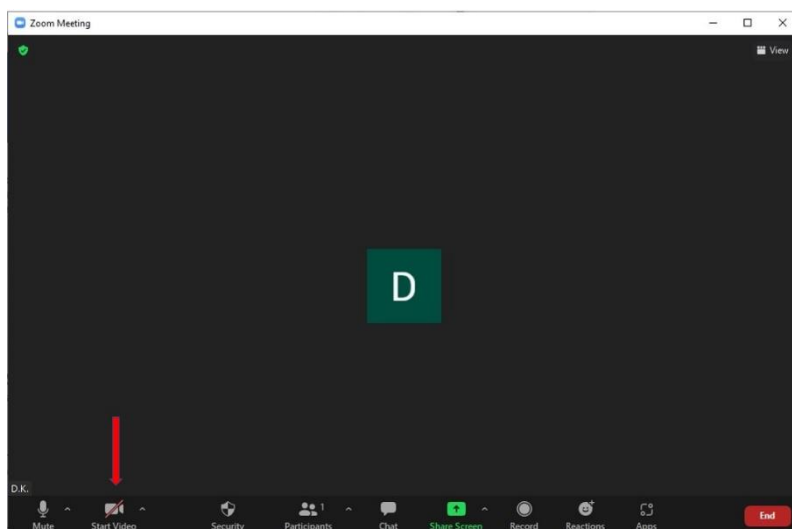
Speakers/chairs can enable their microphone during their presentation by clicking the Unmute button on the left bottom side of the platform.
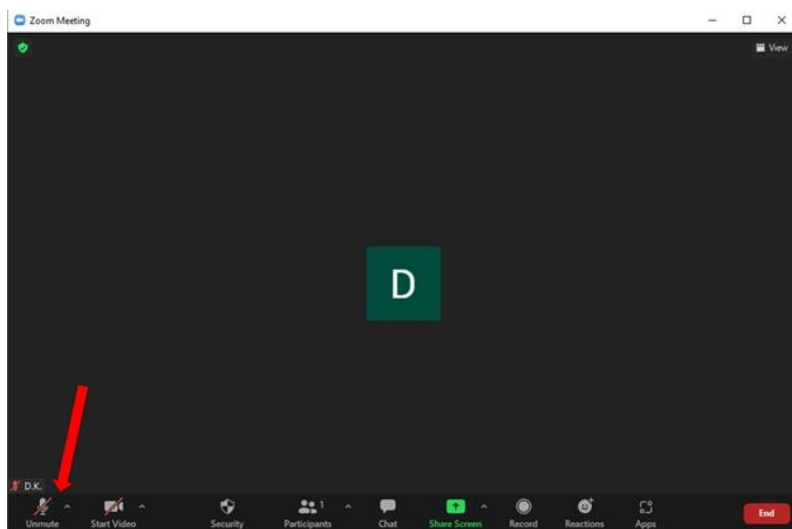
Screen sharing:

Speakers can share their screen using the Share screen button to answer a specific question while navigating through their power point presentation.
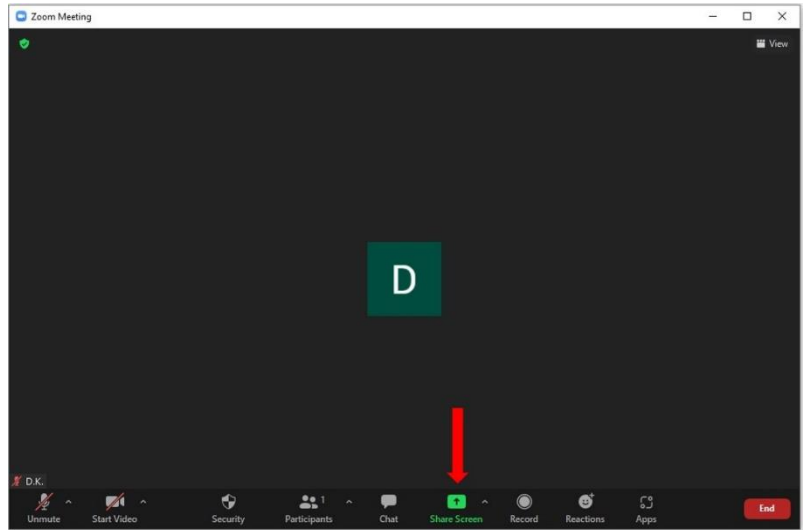
You can share only the presentation and not the whole screen of your personal computer